Title
APOE4 leads to blood-brain barrier dysfunction predicting cognitive decline.

Permalink

Journal

ISSN

Authors
Montagne, Axel
Nation, Daniel A
Sagare, Abhay P
et al.

Publication Date

DOI

Peer reviewed

APOE4 leads to blood-brain barrier dysfunction predicting cognitive decline

Axel Montagne[1,20], **Daniel A. Nation**[1,2,3,4,20], **Abhay P. Sagare**[1,20], **Giuseppe Barisano**[1,20], **Melanie D. Sweeney**[1,20], **Ararat Chakhoyan**[1], **Maricarmen Pachicano**[1], **Elizabeth Joe**[2,5], **Amy R. Nelson**[1], **Lina M. D'Orazio**[2,5], **David P. Buennagel**[6], **Michael G. Harrington**[6], **Tammie L. S. Benzinger**[7,8], **Anne M. Fagan**[8,9,10], **John M. Ringman**[2,5], **Lon S. Schneider**[2,5,11], **John C. Morris**[9,10], **Eric M. Reiman**[12], **Richard J. Caselli**[13], **Helena C. Chui**[2,5], **Julia TCW**[14,15], **Yining Chen**[1], **Judy Pa**[2,16], **Peter S. Conti**[17], **Meng Law**[2,18,19], **Arthur W. Toga**[2,16], **Berislav V. Zlokovic**[1,2,*]

[1]Department of Physiology and Neuroscience, Zilkha Neurogenetic Institute, Keck School of Medicine, University of Southern California, Los Angeles, CA, USA

[2]Alzheimer's Disease Research Center, Keck School of Medicine, University of Southern California, Los Angeles, CA, USA

[3]Department of Psychological Science, University of California, Irvine, CA, USA

[4]Institute for Memory Disorders and Neurological Impairments, University of California, Irvine, CA, USA

[5]Department of Neurology, Keck School of Medicine, University of Southern California, Los Angeles, CA, USA

[6]Huntington Medical Research Institutes, Pasadena, CA, USA

[7]Department of Radiology, Washington University School of Medicine, St. Louis, MO, USA

[*]zlokovic@usc.edu.

[8]The Hope Center for Neurodegenerative Disorders, Washington University School of Medicine, St. Louis, MO, USA

[9]Department of Neurology, Washington University School of Medicine, St. Louis, MO, USA

[10]The Knight Alzheimer's Disease Research Center, Washington University School of Medicine, St. Louis, MO, USA

[11]Department of Psychiatry and Behavioral Sciences, University of Southern California, Los Angeles, CA, USA

[12]Banner Alzheimer Institute, Phoenix, AZ, USA

[13]Department of Neurology, Mayo Clinic, Scottsdale, AZ, USA

[14]Department of Neuroscience & Friedman Brain Institute, Icahn School of Medicine at Mount Sinai, New York, NY, USA

[15]Ronald M. Loeb Center for Alzheimer's disease, Icahn School of Medicine at Mount Sinai, New York, NY, USA

[16]Laboratory of Neuro Imaging, USC Stevens Neuroimaging and Informatics Institute, Keck School of Medicine, University of Southern California, Los Angeles, CA, USA

[17]Molecular Imaging Center, Department of Radiology, Keck School of Medicine, University of Southern California, Los Angeles, CA, USA

[18]Department of Neurological Surgery, Keck School of Medicine, University of Southern California, Los Angeles, CA, USA

[19]Department of Neuroscience and Radiology, Monash University, Alfred Health, Melbourne, VIC, Australia

[20]These authors contributed equally: Axel Montagne, Daniel A. Nation, Abhay P. Sagare, Giuseppe Barisano, Melanie D. Sweeney

Introductory Paragraph

Vascular contributions to dementia and Alzheimer's disease are increasingly recognized[1–6]. Recent studies have suggested that blood-brain barrier breakdown is an early biomarker of human cognitive dysfunction[7], including the early clinical stages of Alzheimer's disease[5,8–10]. Apolipoprotein E4 (*APOE4*), the major Alzheimer's disease susceptibility gene[11–14], leads to accelerated blood-brain barrier breakdown and degeneration of brain capillary pericytes[15–19] that maintain blood-brain barrier integrity[20–22]. Whether *APOE4* cerebrovascular effects contribute to cognitive impairment remains, however, largely unknown. Here we show that *APOE4* carriers (ε3/ε4 and ε4/ε4) are distinguished from non-carriers (ε3/ε3) by blood-brain barrier breakdown in the hippocampus and medial temporal lobe. This finding is apparent in cognitively unimpaired *APOE4* carriers, more severe in those with cognitive impairment, but not related to cerebrospinal fluid or positron emission tomography measurements of Alzheimer's amyloid-β or tau pathology[23]. Indeed, high baseline cerebrospinal fluid levels of the blood-brain barrier pericyte injury biomarker soluble platelet-derived growth factor receptor-β[7,8] predicted future cognitive decline in

APOE4 carriers but not in non-carriers, even after controlling for amyloid-β and tau status, and were correlated with increased activity of blood-brain barrier degrading cyclophilin A-matrix metalloproteinase-9 pathway[19] in cerebrospinal fluid. Our findings suggest that blood-brain barrier breakdown contributes to *APOE4* associated cognitive decline, does so independently of Alzheimer's disease pathology, and might be a therapeutic target in *APOE4* carriers.

The analysis of blood-brain barrier (BBB) permeability by dynamic contrast-enhanced magnetic resonance imaging (DCE-MRI)[7,8] (Fig. 1a; see Methods) in 245 participants (Extended Data Table 1) indicated BBB breakdown in the hippocampus (HC) and parahippocampal gyrus (PHG) in cognitively normal *APOE4* (ε3/ε4 and ε4/ε4) carriers compared to cognitively normal *APOE3* homozygotes (ε3/ε3) both with clinical dementia rating (CDR) score of 0. The BBB breakdown in HC and PHG in *APOE4* carriers further increases with cognitive impairment at CDR=0.5 (Fig. 1b–d). This increase was independent of cerebrospinal fluid (CSF) Aβ and tau changes (Fig. 1e–h), *i.e.*, whether individuals were Aβ+ or Aβ– and pTau+ or pTau– using the accepted cut-off values[7,24,25] (see Methods), where Aβ+ and pTau+ status indicates classical AD pathways[23]. In contrast, *APOE3* carriers developed less pronounced BBB changes in HC and PHG with cognitive impairment (Fig. 1b–d). No significant BBB changes were found in other gray or white matter brain regions in *APOE4* carriers compared to *APOE3* homozygotes, except for increased BBB permeability in the caudate nucleus, and minor leaks in the frontal cortex and corpus callosum in cognitively normal *APOE4* carriers (Extended Data Fig. 1). These findings hold when cognitive dysfunction was evaluated by neuropsychological performance (see Methods) (Extended Data Figs. 2 and 3).

HC and PHG volumes decreased with cognitive impairment in *APOE4*, but not *APOE3* carriers (Fig. 1i–k). The BBB breakdown in HC and PHG in *APOE4* carriers, but not *APOE3* homozygotes, remained a highly significant predictor of cognitive impairment after statistically controlling for age, sex, education, CSF Aβ and pTau status, and HC and PHG volumes, as shown by the estimated marginal means from the analysis of covariance (ANCOVA) models (Fig. 1l,m), and confirmed by logistic regression models (Supplementary Information Table 1). The BBB dysfunction (Fig. 1c,d,l,m) preceded brain atrophy (Fig. 1j,k) and was independent of systemic vascular risk factors (Extended Data Fig. 4).

Because Aβ and tau can both lead to blood vessel abnormalities and BBB breakdown[3,26,27], in a subset of 74 and 96 participants (Extended Data Tables 2a,b), respectively, we studied whether BBB disruption in *APOE4* carriers is downstream to amyloid and tau accumulation. Voxel-based analysis of brain uptake of amyloid by positron emission tomography (PET) indicated a substantially higher accumulation in the orbital frontal cortex (OFC) in cognitively normal *APOE4* carriers compared to *APOE3* homozygotes, as reported[28], but failed to detect accumulation of tau tracer in either *APOE4* or *APOE3* carriers (Extended Data Fig. 5a–d). To determine how BBB permeability relates to amyloid and tau accumulation, we selected 5-mm thick coronal slices in regions of interest including the HC and PHG, where BBB disruption is seen first in *APOE4* carriers compared to *APOE3* homozygotes (Fig. 1b,d,e), OFC, where amyloid accumulation develops initially in *APOE4*

carriers, and inferior temporal gyrus (ITG), a region affected early by tau pathology[29] (Extended Data Fig. 5b,d,e).

Brain uptake of amyloid and tau tracers (after correction for the choroid plexus off-target binding for tau tracer; see Methods and Extended Data Fig. 5f,g) indicated no difference between *APOE4* and *APOE3* carriers in HC, although uptake of both tracers was modestly increased (Fig. 2a,b). BBB disruption in HC in *APOE4* carriers compared to *APOE3* homozygotes (Fig. 2c) was consistent with our findings in the larger cohort (Fig. 1b,c). There was no difference in amyloid and tau accumulation in PHG between *APOE4* carriers and *APOE3* homozygotes, despite BBB disruption in *APOE4* carriers (Fig. 2d–f). There was a higher amyloid accumulation in OFC in cognitively normal *APOE4* compared to *APOE3* carriers (Fig. 2g,h), but no changes in BBB integrity (Fig. 2g,i). There was no change in ITG tau accumulation or BBB integrity in *APOE*4 compared to *APOE3* carriers (Fig. 2j–l). Altogether, these data suggest that BBB disruption in HC and PHG in *APOE4* carriers is independent of AD pathology, and that BBB breakdown in *APOE4* carriers starts in the medial temporal lobe, a region responsible for memory encoding and other cognitive functions.

Elevated cerebrospinal fluid (CSF) levels of soluble platelet-derived growth factor receptor-β (sPDGFRβ) in humans and animal models indicate pericyte injury linked to BBB breakdown[7,8,30] and cognitive dysfunction[7,30]. Using a median split for visual display of the CSF sPDGFRβ baseline levels from 350 participants (see Methods), we stratified all participants into two groups, with low CSF sPDGFRβ levels (0-600 ng/mL, *grey*), and high sPDGFRβ levels (600-2,000 ng/mL, *blue*) (Fig. 3a). Our data in 146 *APOE4* carriers and *APOE3* homozygotes evaluated by cognitive exams over two-year intervals up to 4.5 years from baseline show that participants with higher baseline CSF sPDGFRβ levels exhibited accelerated cognitive decline on global mental status exam and global cognitive composite z-scores, which remained significant after controlling for CSF Aβ and tau status (Fig. 3b,c; Supplementary Information Table 2). When stratified by *APOE* status, higher baseline CSF sPDGFRβ levels in *APOE4* carriers predicted cognitive decline after controlling for CSF Aβ and pTau status (Fig. 3d,e; Supplementary Information Table 3), but did not predict decline in *APOE3* homozygotes (Fig. 3f,g; Supplementary Information Table 4).

The increase in CSF sPDGFRβ with cognitive impairment was also found on cross-sectional CDR analysis in *APOE4*, but not *APOE3* carriers (Fig. 4a–b; Extended Data Table 3; Supplementary Information Table 5). Increased CSF levels of sPDGFRβ in *APOE4* carriers correlated with increases in BBB permeability in HC and PHG (Fig. 4c,d), and elevated levels of molecular biomarkers of BBB breakdown including albumin CSF/plasma quotient, and CSF fibrinogen and plasminogen (Fig. 4e–g).

Next, we focused on proinflammatory cyclophilin A-matrix metalloproteinase-9 (CypA-MMP9) pathway that when activated by brain capillary pericytes in *APOE4*, but not *APOE3*, knock-in mice leads to MMP9-mediated BBB breakdown, which in turn leads to neuronal stress related to leaked blood-derived neurotoxic proteins followed by neuronal dysfunction and loss of synaptic proteins[19]. Activation of CypA-MMP9 pathway was also noted by brain issue analysis in degenerating brain capillary pericytes in *APOE4* compared

to *APOE3* AD carriers[16]. Here, we found that living *APOE4* carriers, but not *APOE3* homozygotes, develop an increase in CypA CSF levels with cognitive impairment (Fig. 4h,i), which correlated with elevated CSF sPDGFRβ (Fig. 4j). *APOE4*, but not *APOE3* carriers, had also elevated MMP9 CSF levels with cognitive impairment (Fig. 4k), which correlated with elevated CSF CypA levels (Fig. 4l), suggesting that activation of CypA-MMP9 pathway in *APOE4* carriers correlates with pericyte injury similarly as shown in animal models[19]. There were no differences in glia, other inflammatory, and endothelial cell injury CSF biomarkers between impaired and unimpaired *APOE4* and *APOE3* participants, but there was an increase in neuron-specific enolase with cognitive impairment in *APOE4* carriers confirming neuronal stress (Extended Data Fig. 6), consistent with HC and PHG atrophy (Fig. 1j,k).

Studies in *APOE* knock-in mice and mouse pericytes have shown that apoE3, but not apoE4, inhibits CypA via low-density lipoprotein receptor-related protein 1 transcriptionally, which in turn inhibits MMP9 transcriptionally[19]. Consistent with the mouse data, human induced pluripotent stem cells-derived *APOE4* (ε4/ε4) compared to *APOE3* (ε3/ε3) pericytes had substantially higher levels of CypA and secreted MMP9 (Fig. 4m,n) suggesting that apoE may control the CypA-MMP9 pathway in human pericytes in an isoform-specific manner similar as in mouse models[19].

APOE4 compared to *APOE3* reduced CSF Aβ$_{1-42}$ and increased CSF pTau levels with cognitive impairment (Extended Data Fig. 7) as reported[23], which remained significant after controlling for CSF sPDGFRβ levels (Extended Data Fig. 7). All together these findings support that Aβ and tau pathways operate independently of the BBB breakdown pathway during early stages of cognitive impairment in *APOE4* carriers.

In summary, we show that *1*) BBB breakdown contributes to cognitive decline in *APOE4* carriers independent of AD pathology; *2*) high baseline CSF levels of sPDGFRβ can predict future cognitive decline in *APOE4* carriers; and *3*) *APOE4*, but not *APOE3*, activates the CypA-MMP9 pathway in CSF, which may lead to accelerated BBB breakdown causing neuronal and synaptic dysfunction[19]. Since blockade of the CypA-MMP9 pathway in *APOE4* knock-in mice restores BBB integrity followed by normalization of neuronal and synaptic functions[19], one can consider that CypA inhibitors (some of which have been used in humans for non-neurological applications[31]) might also suppress the CypA pathway in cerebral blood vessels in *APOE4* carriers that should improve cerebrovascular integrity, and the associated neuronal and synaptic deficits, slowing down cognitive impairment.

Methods

Study Participants

Participants were recruited from three sites, including the University of Southern California (USC), Los Angeles, CA, Washington University (WashU), St. Louis, MO, and Banner Alzheimer's Institute Phoenix, AZ and Mayo Clinic Arizona, Scottsdale, AZ as a single site. At the USC site, participants were recruited through the USC Alzheimer's Disease Research Center (ADRC): combined USC and the Huntington Medical Research Institutes (HMRI), Pasadena, CA. At the WashU site, participants were recruited through the Washington

University Knight ADRC. At Banner Alzheimer's Institute and Mayo Clinic Arizona site, participants were recruited through the Arizona Apolipoprotein E (*APOE*) cohort. The study and procedures were approved by the Institutional Review Boards of USC ADRC, Washington University Knight ADRC, and Banner Good Samaritan Medical Center and Mayo Clinic Scottsdale indicating compliance with all ethical regulations. Informed consent was obtained from all participants prior to study enrollment. All participants (n=435) underwent neurological and neuropsychological evaluations performed using the Uniform Data Set (UDS)[32] and additional neuropsychological tests, as described below, and received a venipuncture for collection of blood for biomarker studies. A lumbar puncture (LP) was performed in 350 participants (81%) for collection of cerebrospinal fluid (CSF). The dynamic contrast-enhanced magnetic resonance imaging (DCE-MRI) for assessment of blood-brain barrier (BBB) permeability was performed in 245 participants (56%) who had no contraindications for contrast injection. Both LP and DCE-MRI were conducted in 172 participants. Among the 245 DCE-MRI participants, 74 and 96 were additionally studied for brain uptake of amyloid and tau PET radiotracers, respectively, as described below. All biomarker assays, MRI, and PET scans were analyzed by investigators blinded to the clinical status of the participant.

Participant Inclusion and Exclusion Criteria

Included participants (≳45 years of age) were confirmed by clinical and cognitive assessments to be either cognitively normal or at the earliest symptomatic stage of Alzheimer disease. A current or prior history of any neurological or psychiatric conditions that might confound cognitive assessment, including organ failure, brain tumors, epilepsy, hydrocephalus, schizophrenia, and major depression, was exclusionary. Participants were stratified by *APOE* genotype as *APOE4* carriers (ε3/ε4 and ε4/ε4) and *APOE4* non-carriers (ε3/ε3) also defined as *APOE3* homozygotes who were cognitively normal or with mild cognitive dysfunction, as determined by clinical dementia rating (CDR) scores[33] and the presence of cognitive impairment in one or more cognitive domains based on comprehensive neuropsychological evaluation including performance on ten neuropsychological tests assessing memory, attention/executive function, language and global cognition. For all analyses individuals with ε3/ε4 and ε4/ε4 alleles were pooled together in a single *APOE4* group, as we did not find in the present cohort consisting of 82-86% ε3/ε4 and 14-18% ε4/ε4 participants (depending on the outcome measure) a significant difference between the two versus one ε4 allele for the studied parameters including the BBB permeability unidirectional transfer constant K_{trans} values and sPDGFRβ CSF values (see statistical section below). Individuals have been additionally stratified by Aβ and pTau CSF analysis as either Aβ-positive (Aβ$_{1-42}$+, <190 pg/mL) or Aβ-negative (Aβ$_{1-42}$-, >190 pg/mL), or pTau-positive (pTau+, >78 pg/mL) or pTau-negative (pTau−, <78 pg/mL), using accepted cutoff values[7,24,25].

Participants were excluded if they were diagnosed with vascular cognitive impairment or vascular dementia. Clinical diagnoses were made by neurologists and criteria included whether the patient 1) had a known vascular brain injury and 2) the clinician judged that the vascular brain injury played a role in their cognitive impairment, and/or pattern and course of symptoms. In addition to clinical diagnosis, presence of vascular lesions was confirmed

by moderate-to-severe white matter changes and lacunar infarcts by fluid-attenuated inversion recovery (FLAIR) MRI and/or subcortical microbleeds by T2*-weighted MRI[1]. Participants were also excluded if they were diagnosed with Parkinson's disease, Lewy body dementia or frontotemporal dementia. History of a single stroke or transient ischemic attack was not an exclusion unless it was related to symptomatic onset of cognitive impairment. Participants also did not have current contraindications to MRI and were not currently using medications that might better account for any observed cognitive impairment.

Clinical Exam

Participants underwent clinical assessments according to UDS procedures harmonized across all study sites, including clinical interview and review of any neurocognitive symptoms and health history with the participant and a knowledgeable informant. A general physical and neurologic exam was conducted. The CDR assessment was conducted in accordance with published standardization procedures, including standardized interview and assessment with the participant and a knowledgeable informant. In accordance with current diagnostic models for cognitive and biological research criteria for cognitive impairment and AD[23], participants were separately stratified by cognitive impairment and AD biomarker abnormality using established cutoffs for CSF $A\beta_{1-42}$ and pTau[7,24,25]. Cognitive impairment was determined based on global CDR score and neuropsychological impairment in one or more cognitive domains.

Vascular Risk Factors

The vascular risk factor (VRF) burden in each participant was evaluated through physical examination, blood tests, and clinical interviews with the participant and informant; history of cardiovascular disease (heart failure, angina, stent placement, coronary artery bypass graft, intermittent claudication), hypertension, hyperlipidemia, type 2 diabetes, atrial fibrillation, and transient ischemic attack or minor stroke were investigated. The total VRF burden was defined by the sum of these risk factors, as previously described[7]. We assigned an elevated VRF burden to individuals with 2 or more VRFs. This threshold was adopted based on previous studies showing that the presence of two or more VRFs is associated with occult cerebrovascular disease at autopsy in older adults with AD, whereas a single VRF is common and not necessarily associated with increased cerebrovascular disease in this population[34,35].

Cognitive Domain Impairment Evaluation

Impairment in one or more cognitive domains was based on performance on comprehensive neuropsychological testing, using previously described neuropsychological criteria for cognitive impairment[7]. All participants underwent neuropsychological testing that included the UDS battery (version 2.0 or 3.0) plus supplemental neuropsychological tests at each site. Raw test scores were converted to age-, sex- and education-corrected z-scores using the National Alzheimer's Coordinating Center (NACC) regression-based norming procedures (www.alz.washington.edu). Normalized z-scores from a total of 10 neuropsychological tests were evaluated in determining domain impairment, including three tests per cognitive domain (memory, attention/executive function and language) and one test of global cognition. Impairment in one or more cognitive domains was determined using previously

described neuropsychological criteria, and was defined as a score >1 standard deviation (SD) below norm-referenced values on two or more tests within a single cognitive domain or three or more tests across cognitive domains[36]. Prior studies have established improved sensitivity and specificity of these criteria relative to those employing a single test score, as well as adaptability of this diagnostic approach to various neuropsychological batteries[36,37]. Participants were excluded from cognitive domain analyses if they had less than 90% complete neuropsychological test data (*i.e.*, 53, 24, and 82 participants were excluded for MRI, PET, and CSF analyses, respectively). Included participants were classified as 0, 1, or 2+ based on the number of cognitive domains with two or more impaired test scores.

Test battery specifics for each UDS version and recruitment site are as follows. *i*) Global cognition: MMSE for UDS version 2[38] and MoCA for UDS version 3[39]. *ii*) Memory: The Logical Memory Story A Immediate and Delayed free recall tests [modified from the original Wechsler Memory Scales – Third Edition (WMS-III)] for UDS version 2 and the Craft Stories Immediate and Delayed free recall for UDS version 3. For supplemental tests the USC participants underwent the California Verbal Learning Test – Second Edition (CVLT-II) and the Selective Reminding Test (SRT) sum of free recall trials. Norm-referenced scores for these supplemental test scores were derived from a nationally representative sample published with the test manual (CVLT-II)[40] and in studies of normally aging adults (SRT). *iii*) Attention and executive function: The Trails A, Trails B, and Wechsler Adult Intelligence Scale - Revised (WAIS-R) Digit Span Backwards tests for UDS version 2 and the Trails A, Trails B and Digit Span Backwards tests for UDS version 3. *iv*) Language: The Animal Fluency, Vegetable Fluency, and Boston Naming Tests for UDS version 2 and Animal Fluency, Vegetable Fluency, and Multilingual Naming Test (MINT) for UDS version 3.

Magnetic Resonance Imaging and Analysis

The MRI data sets were obtained at Mark and Mary Stevens Neuroimaging and Informatics Institute of USC and Washington University of St. Louis. We developed a standardized high-resolution 3T MR imaging brain scan protocol. For USC site, a Siemens 3T Prisma scanner was used with a product 32-channel head receive coil and body transmit coil. For WashU site, a Siemens 3T mMR with 20-channel head coil and Siemens 3T Vida with 64-channel head coil were used. Anatomical coronal spin echo T2-weighted scans were first obtained through the hippocampi (TR/TE 8020/50 ms, NEX = 1, slice thickness 2 mm with 2 mm gap between slices, FOV = 175 x 175 mm, matrix size = 448 x 448). Baseline coronal T1-weighted maps were then acquired using a T1-weighted 3D volumetric interpolated breath-hold sequence (VIBE) sequence and variable flip angle method using flip angles of 2°, 5°, 10°, 12°, and 15°. Coronal DCE-MRI covering the hippocampi and temporal lobes were acquired using a T1-weighted 3D VIBE sequence (FA = 15°, TR/TE = 5.14/2.18 ms, NEX = 1, slice thickness 5 mm with no gap, FOV 175 x 175 mm, matrix size 320 x 320, voxel size was $0.550 \times 0.550 \times 5$ mm^3). This sequence was repeated for a total of 16 min with an approximate time resolution of 15.4 sec. Gadolinium-based contrast agent (GBCA), Gadoterate meglumine (Dotarem®, Guerbet, France) (0.05 mmol/kg), was administered intravenously into the antecubital vein using a power injector, at a rate of 3 mL/s followed by a 25 mL saline flush, 30 s into the DCE scan.

The standardization and optimization of the MRI protocol required several tests performed on a phantom. Specifically, scanner characterization and calibration sequences including B_0, T1, and variable flip-angle mapping were implemented, optimized, and applied. After the achievement of good results in terms of quality control and reproducibility, we standardized and employed the same pre-contrast and dynamic T1-weighted protocols at both USC and Washington University sites. Of note, all the other MR sequences were identical too on both scanners.

In order to minimize the inter-site variability, the entire MRI protocol including the anatomical and DCE pulse sequences were 100% mirrored from one site to another. To minimize inter-site variability, the same contrast agent Gadoterate meglumine (Dotarem®) were injected to participants at the same concentration (0.05 mmol/kg). Finally, the same exact pre- and post-processing analysis pipeline was applied for both sites which includes T1 multi-FA mapping using linear fitting and Patlak-based DCE modeling using the arterial input function determined in each individual from the internal carotid artery. Applying all the above cited factors significantly limited inter-site variability.

The consistency of the results from the two sites has been additionally confirmed by our previous publication[7]. In brief, we performed the analysis of the combined DCE datasets from both USC and WashU sites, and additionally site-specific analysis for each of the two sites separately, which showed no statistically significant differences across sites. Recently, we invited a subset of 52 participants for an additional T1-weighted scan without contrast (using the same scanner and same MR pulse sequences) after their first DCE-MRI[41] and measured both B_0 and T1 values at 2-year interval. This study showed that the results were unchanged and consistent across the scans, supporting minimal intra-site variability.

Quantification of the Blood-Brain Barrier Permeability

See Supplementary Information, Supplementary Methods.

Quantification of Regional Brain Volumes

HC and PHG morphometry were performed using the FreeSurfer (v5.3.0) software package[42] (http://surfer.nmr.mgh.harvard.edu/), as previously performed[7]. HC and PHG were segmented using FreeSurfer Desikan-Killiany and subcortical atlases[43,44]. Then, regional volumes (mm^3) were derived accordingly. The technical details of this procedure are described in previous publications[45,46]. Data processing and visualization were performed using the Laboratory of Neuro Imaging (LONI) pipeline system (http://pipeline.loni.usc.edu) and Quantitative Imaging Toolkit[47–49].

Positron Emission Tomography and Analysis

The PET image acquisition was performed at the Molecular Imaging Center of USC or Mallinckrodt Institute of Radiology of WashU. Amyloid and tau PET studies were conducted using ^{18}F-Florbetaben (FBB) or ^{18}F-Florbetapir (FBP) and ^{18}F-Flortaucipir (AV1451), respectively. FBB (Life Molecular Imaging, Inc.) was obtained from SOPHIE, Inc. for USC site, while FBP was provided by Eli Lilly and Company for WashU site. For all amyloid PET analysis FBP and FBB datasets were combined. AV1451 was provided by

Avid Radiopharmaceuticals, Inc. for USC site and was produced by the Mallinckrodt Institute of Radiology for WashU site. A Siemens Biograph 64 PET scanner was used at USC site. At WashU site, FBP scans were acquired on a Siemens mMR and AV1451 scans were acquired on a Siemens Biograph mCT. The mCT session was used for attenuation correction of the mMR scans. Participants were injected with 300 MBq (±10%) of FBB or 370 MBq (±10%) of FBP. FBB and FBP images were acquired from 90 to 110 min and 50 to 70 min, respectively, after injection in accordance with the manufacturers' recommendation. Individuals who participated in amyloid and tau PET studies also had their DCE-MRI scan within a 2.2 ± 0.9 and 2.1 ± 0.6 month period of their amyloid and tau PET scans, respectively.

Briefly, a computed tomography (CT) scan was performed first for attenuation correction before each PET imaging session. The downloaded PET images from FBB, FBP, and AV1451 tracers were processed by using standard uptake value maps (SUV in g/mL). All PET images were co-registered to structural high-resolution 3D T1-weighted Magnetization Prepared Rapid Acquisition Gradient Echo (MP-RAGE) MRI images using FSL-FLIRT (FMRIB's Linear Image Registration Tool)[50]. FreeSurfer-segmented cerebellum was used as a reference tissue to normalize for both amyloid and tau[51].

After co-registration of PET images into an anatomical reference image (MNI152 standard-space), the Statistical Parametric Mapping (SPM12) was used for group comparison in a voxel-by-voxel basis. Age at time of PET imaging session, sex, and education were introduced in a multiple regression model as covariates. Level of significance was set to $p<0.001$ for amyloid and $p<0.005$ for tau (uncorrected p values) with the minimum number of voxels (Ke) in a cluster of 50.

Additionally, given the known AV1451 off-target ligand binding in the choroid plexus (CP)[52,53], which can contribute to HC regional AV1451 signal due to close proximity of CP to HC and relatively low spatial resolution of PET scans (*i.e.*, ~6-mm voxel size), we took advantage of visualizing CP by DCE-MRI, also performed in these individuals, that allowed us to subtract contribution of the CP signal to the HC AV1451 proper signal. The following steps were employed to correct for off-target ligand binding to CP (see Extended Data Fig. 5): *Step 1*) HC masks were generated from the 3D T1-weighted MP-RAGE; *Step 2*) CP masks were generated from the T1-weighted VIBE image post-GBCA (FA = 15°) image; *Step 3*) HC and CP masks were overlaid; and *Step 4*) CP overlap with HC mask was subtracted to obtain CP-corrected HC PET signal after adding 6-mm voxel size on top of CP mask generated from DCE data. Representative images of HC AV1451 PET signal before and after applying the CP correction are shown in Extended Data Fig. 5.

We next quantified regional changes in amyloid and tau SUV ratio (SUVR) in relation to regional DCE-MRI K_{trans} values in all participants stratified by *APOE* genotype. The regional SUVR values were taken from the FreeSurfer-segmented HC, PHG, OFC[28], and ITG[29]. The BBB K_{trans} constant (DCE-MRI) was determined in all participants (Extended Data Tables 2a,b). This includes those who received both amyloid and tau (n=58), only amyloid (n=9) or only tau (n=29).

Lumbar Puncture and Venipuncture

Participants underwent a lumbar puncture and venipuncture in the morning after an overnight fast. The CSF was collected in polypropylene tubes, processed (centrifuged at 2,000 g, 4°C, 10 min USC site; 5 min WashU site), aliquoted into polypropylene tubes and stored at −80°C until assay. Blood was collected into ethylenediaminetetraacetic acid (EDTA) tubes and processed (centrifuged at 2000 g, 4°C, 10 min USC site; 5 min WashU site). Plasma and buffy coat were aliquoted in polypropylene tubes and stored at −80°C; buffy coat was used for DNA extraction and *APOE* genotyping.

APOE Genotyping

DNA was extracted from buffy coat using the Quick-gDNA Blood Miniprep Kit (Catalog no. D3024, Zymo Research, Irvine, CA). *APOE* genotyping was performed via polymerase chain reaction (PCR)-based retention fragment length polymorphism analysis, as previously reported[7].

Molecular Assays

Quantitative Western Blotting of sPDGFRβ—The quantitative Western blot analysis was used to detect sPDGFRβ in human CSF (ng/mL), as we previously reported[7,8].

BBB Breakdown Biomarkers—Albumin quotient (Qalb the ratio of CSF-to-plasma albumin levels) and CSF levels of fibrinogen and plasminogen were determined using enzyme-linked immunosorbent assay (ELISA), as we previously reported[7,8].

Cyclophilin A (CypA)—We developed a novel CypA assay on the Meso Scale Discovery (MSD) platform. Standard-bind 96-well plates (Catalog no. L15XA-3 / L11XA-3, MSD, Rockville, MD) were spot-coated with 5 μL per well of 40 μg/mL rabbit polyclonal cyclophilin A antibody (Catalog no. 10436-T52, Sino Biological, Wayne, PA) prepared in 0.03% Triton X-100 in 0.01 M PBS pH 7.4 solution. The plates were left undisturbed overnight to dry at room temperature. The next day, the plates were blocked with 150 μL per well of Blocking One (Catalog no. 03953-95, Nacalai Tesque, Japan) and incubated for exactly one hour with shaking. Meanwhile, samples and standards were prepared in Blocking One blocking buffer. Different concentrations ranging from 3.5-200 ng/mL of a recombinant human cyclophilin A protein (Catalog no. 3589-CAB, R&D Systems, Minneapolis, MN) were used to generate a standard curve. All CSF samples were diluted 1:3. After blocking, the plates were manually washed 3 times with 200 μL per well of wash buffer (in 0.05% Tween-20 in 0.01 M PBS pH 7.4). The prepared samples or standards were added at 25 μL per well, and the plates were incubated overnight at 4°C with shaking.

The next day, the plates were washed 3 times, and 25 μL per well of 1 μg/mL sulfo-tagged mouse monoclonal cyclophilin A detection antibody (Catalog no. ab58144, Abcam, Cambridge, MA), prepared in Blocking One. The plates were incubated for 90 min at room temperature with shaking. Next, plates were washed 4 times, then 150 μL per well of 2x Read Buffer T with surfactant (Catalog no. R92TC-3, MSD, Rockville, MD) was added and the plates were read immediately on the MSD SECTOR Imager 6000 (MSD, Rockville, MD) with electrochemiluminescence detection.

The raw readings were analyzed by subtracting the average background value of the zero standard from each recombinant standard and sample readings. A standard curve was constructed by plotting the recombinant standard readings and their known concentrations and applying a nonlinear four-parameter logistics curve fit. The CypA concentrations were calculated using the samples' reading and the standard curve equation; the result was corrected for the sample dilution factor to arrive at the CypA concentration in the CSF samples.

Matrix Metalloproteinase-9 (MMP9)—CSF levels of MMP9 were determined using human MMP9 Ultra-Sensitive Kit from MSD (Cat. No. K151HAC).

Neuron-Specific Enolase—CSF levels of neuron-specific enolase (NSE) were determined using ELISA (Cat. No. E-80NEN, Immunology Consultant Laboratories, Portland, OR). The company no longer sells this product; thus, this analyte has been measured in a majority of participants but not in individuals that most recently enrolled in the study.

S100B—CSF levels of the astrocyte-derived cytokine, S100 calcium-binding protein B (S100B), were determined using ELISA (Cat. No. EZHS100B-33K, EMD Millipore, Billerica, MA).

Inflammatory Markers—MSD multiplex assay was used to determine CSF levels of intercellular adhesion molecule 1 (ICAM1) (Cat. No. K15198D, MSD, Rockville, MD), and interleukin-6 (IL6), IL-1β, tumor necrosis factor α (TNFα), and interferon gamma (IFNγ) (Cat. No. K15049G, MSD, Rockville, MD).

Aβ Peptides—MSD multiplex assay (Cat. No. K15200E, MSD, Rockville, MD) was used to determine CSF levels of Aβ_{1-42}. Participants were stratified based on CSF analysis as either Aβ_{1-42}-positive (Aβ_{1-42}+, <190 pg/mL) or Aβ_{1-42}-negative (Aβ-, >190 pg/mL) using the accepted cutoff values as previously reported for the MSD 6E10 Aβ peptide assay[24].

Tau—Phosphorylated tau (pT181) was determined by ELISA (Cat. No. 81581, Innotest®, Fujirebio US, Inc., Malvern, PA). Participants were stratified based on CSF analysis as either pTau$_{181}$-positive (pTau+, >78 pg/mL) or pTau$_{181}$-negative (pTau−, <78 pg/mL), using the accepted cutoff value as previously reported[25].

Human Induced Pluripotent Stem Cells (iPSCs)

iPSC lines were generated by reprogramming of *APOE* ε4/ε4 and *APOE* ε3/ε3 control and AD donor skin fibroblasts as recently reported[54]. Reprogramming was performed using integration-free Sendai virus vectors and passaged cells to passage 15 and confirmed normal karyotype. hiPSCs were maintained on Matrigel (Corning) in mTeSR1 (Catalog no. 85850, StemCell Technologies, Vancouver, BC, Canada) supplemented with 10 ng/mL FGF2 StemBeads (StemCultures) or mTeSR plus (StemCell Technologies) every other day.

Differentiation of iPSCs into Pericytes

Differentiation of iPSCs into pericytes was carried out as described previously[55]. Briefly, iPSCs were dissociated with ReLeSR (catalog no. 05872, StemCell Technologies) and seeded at 55,000 cells/cm^2 in Essential 8 medium (Catalog no. A1517001, ThermoFisher, Waltham, MA, USA) supplemented with ROCK inhibitor Y-27632 (10 μM, catalog no. 72304, StemCell Technologies) on Matrigel (0.5 mg/6-well plate, Catalog no. 354230, Corning, NY, USA). After 24 hours incubation, the iPSCs were switched into STEMdiff Mesoderm Induction Medium (MIM, Catalog no. 05221, StemCell Technologies) for 5 days with daily medium change. On day 6 of MIM treatment, the cells were plated on Matrigel at 25,000 cells/cm^2 in Pericyte Medium (Catalog no. 1201, ScienCell, Carlsbad, CA, USA) for an additional 7 days. The differentiated cells were dissociated with Accutase (catalog no. 07920, Stemcell Technologies). Following incubation with human PDGFRβ biotinylated antibody (Catalog no. BAF385, R&D Systems, Minneapolis, MN, USA), the cells were incubated with anti-biotin microbeads (Catalog no. 130-090-485, Miltenyi Biotec, Bergisch Gladbach, NRW, Germany) and magnetically sorted using MACS LS columns (Catalog no. 130-042-401, Miltenyi Biotec) following the manufacturer's instructions. Sorted pericytes were plated at a density of 25,000 cells/cm^2 on Matrigel-coated coverslips for immunocytochemistry analyses or ploy-L-lysine-coated six-well culture plates for Western blot analyses. Differentiated pericytes were positive for pericyte markers PDGFRβ, CD13, and NG2, and negative for endothelial marker CD31, astrocytic marker GFAP, and microglial marker CD11b.

Statistical Analyses

Prior to performing statistical analyses, we first screened for outliers using the Grubbs' test, also called the ESD method (Extreme Studentized Deviate), applying a significance level of α=0.01 (https://www.graphpad.com/quickcalcs/grubbs1/). For each of the outliers identified, a secondary index of outlier influence was applied using the degree of deviation from the mean (greater than +/− 3 SDs)[56]. Using these stringent criteria, a total of 5 outliers one each in main Figure panels 1j, 1k and 2j, and one each in Extended Data Figs. 6a and 6b, were removed from analyses, as indicated in the legends of these figures. Continuous variables were also evaluated for departures from normality through quantitative examination of skewness and kurtosis, in addition to visual inspection of frequency distributions. Where departures of normality were identified, log10-transformations were applied, and distribution normalization was confirmed prior to parametric analyses. This has been done for main Figs. 4h and 4k, and Extended Data Figs. 7a, 7b, 7d, and 7e. Since use of log10-transformations accounts for any non-normality this obviated the need for outliers exclusion.

DCE-MRI K_{trans}, and CSF sPDGFRβ and CypA—Regional DCE-MRI K_{trans} values and CSF sPDGFRβ, CypA and MMP9 levels were compared across the entire sample stratified by *APOE* status. Since in *APOE4* group relatively small number of participants were homozygous ε4/ε4 compared to heterozygous ε3/ε4, *i.e.*, 14% for DCE-MRI analysis, and 18% for sPDGFRβ analysis, and initial comparisons between ε4/ε4 and ε3/ε4 carriers did not show any significant differences in regional HC and PHG DCE-MRI K_{trans} values (CDR 0, p_{HC}=0.19 and p_{PHG}=0.54 (PHG); CDR 0.5, p_{HC}=0.22 and p_{PHG}=0.84) or CSF sPDGFRβ levels (CDR 0, p=0.23; CDR 0.5, p=0.47), all subsequent analyses combined

APOE4 carriers (ε3/ε4 and ε4/ε4), and compared these participants to *APOE3* carriers (ε3/ε3) stratified by cognitive impairment status (CDR 0 vs 0.5 and 0 vs 1 vs 2+ cognitive domains impairment using analysis of covariance (ANCOVA) with false discovery rate (FDR) correction for multiple comparisons (see details below). For CDR analyses, model covariates included age, sex, and education. Cognitive domain impairment was determined using age, sex, and education-corrected values, so these covariates were not additionally included in the analyses. Additional post-hoc ANCOVA analyses evaluated whether observed differences remained significant after stratifying *APOE4* carriers by CSF $A\beta_{1-42}$ and pTau status, and after statistically controlling for CSF $A\beta_{1-42}$ and pTau status and regional brain volume in *APOE4* non-carriers and carriers. These findings were also confirmed by hierarchical logistic regression models using the same covariates.

PET AD Biomarkers—In a subset of participants who underwent amyloid and tau PET imaging together with DCE-MRI studies, we used ANCOVA models controlled for age, sex and education to compare regional amyloid and tau ligand binding and DCE-MRI values in a set of *APOE4* non-carriers and carriers within *a priori* regions of interest, based on prior imaging studies, to determine whether distinct regional pathologies were observed by *APOE4* carrier status.
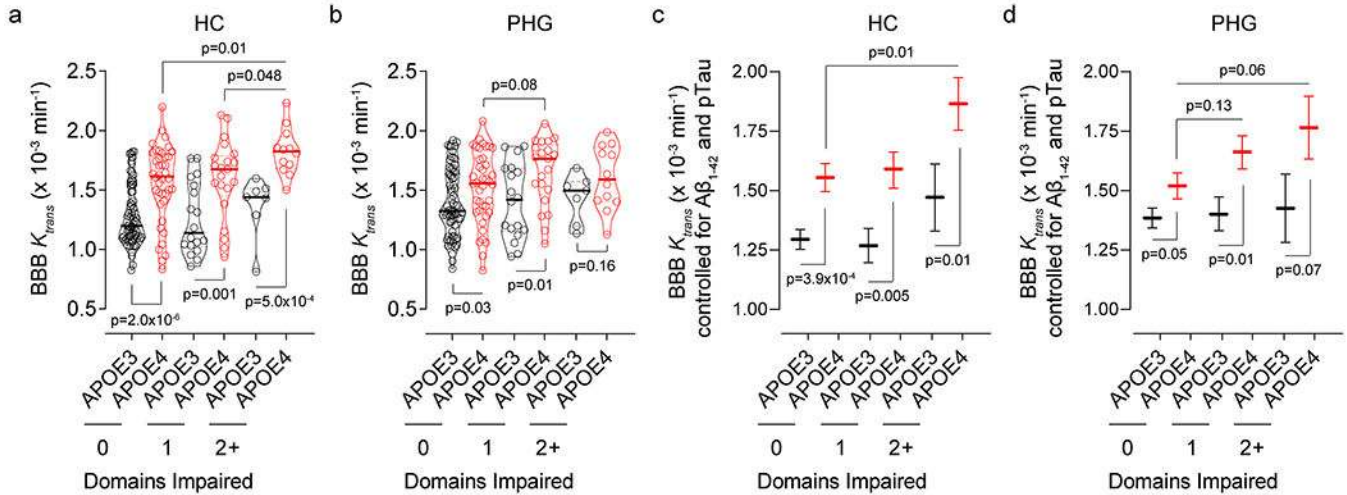
Baseline CSF sPDGFRβ as a continuous predictor of cognitive decline—For linear mixed model analysis, baseline CSF sPDGFRβ was a continuous predictor of demographically-corrected global cognitive change over 2-year follow up intervals, controlling for CSF $A\beta_{1-42}$ and CSF pTau status. Global cognition was indexed by age-, sex-, and education-corrected z-scores on mental status exam (MMSE or MoCA) and as the global cognitive composite of all age-, sex-, and education-corrected neuropsychological test z-scores (see above for list of neuropsychological tests). Time was modeled with date of lumbar puncture as baseline (T_0) with two follow up intervals of 2 years each (T_{1-2}). Additional analyses confirmed all findings when time was modeled as time since baseline, with date of lumbar puncture as baseline (T_0) and follow up as annual intervals (T_{1-n}).

All longitudinal mixed models treated CSF sPDGFRβ as a continuous predictor. Although we have previously established CSF sPDGFRβ as a marker of pericyte injury[7,8,57], the optimal cutoff value for abnormal CSF sPDGFRβ levels indicative of pericyte injury remains unknown. Autopsy studies are required to determine optimal *in vivo* biomarker cutoff values predictive of gold-standard neuropathological measures, such as studies conducted for CSF and PET markers of amyloid and tau. Given the lack of available autopsy data relating CSF sPDGFRβ to neuropathological markers of pericyte injury, we chose to divide participants by CSF sPDGFRβ values using median split for the purposes of visual display only (higher CSF sPDGFRβ was above sample median and lower CSF sPDGFRβ was below sample median). The median split was not used in statistical analyses and was only used for the purpose of visual display (see Figure 3a) for statistical parameters from analyses using CSF sPDGFRβ as a continuous predictor of cognitive decline).

Correlational Analyses—Pearson product moment correlations were used to evaluate relationships among CSF sPDGFRβ, CypA, MMP9, fibrinogen, plasminogen and hippocampal and parahippocampal BBB K_{trans} levels among *APOE4* carriers.

Multiple Comparison Correction and Missing Data—Given the large number of analyses, FDR-correction was applied to p-values for primary study outcomes (*i.e.*, DCE-MRI, sPDGFRβ) evaluated in the entire sample by *APOE4* carrier status and CDR status using the Benjamini-Hochberg method[58] in ANCOVA and logistic regression models controlling for age, sex, education, brain volume, and CSF Aβ$_{1-42}$ and pTau status (for DCE-MRI analyses). Post-hoc confirmatory analyses in participant subsets further evaluating independence of CSF and PET markers of amyloid and tau, evaluation of mechanistic markers (*i.e.*, CypA and MMP9), and longitudinal analysis of predictive value of CSF sPDGFRβ were not multiple comparison corrected. For longitudinal data with variable follow up, we utilized linear mixed model analyses with the account for missing data via the missing at random assumption.

Extended Data

Extended Data Figure 1. Regional BBB K_{trans} constant in eight additional brain regions in *APOE4* carriers and non-carriers (*APOE3*) with CDR status 0 and 0.5.

DCE-MRI BBB permeability, K_{trans} constant, in the inferior temporal gyrus (ITG, **a**), superior frontal gyrus (SFG, **b**), caudate nucleus (CN, **c**), thalamus (Thal, **d**), striatum (Str, **e**), subcortical watershed normal-appearing white matter (Subcort. WS NAWM, **f**), corpus callosum (CC, **g**), and internal capsule (IC, **h**) in CDR 0 *APOE3* (black, n=128) and *APOE4* (red, n=68) carriers, CDR 0.5 *APOE3* (black, n=14) and *APOE4* (red, n=25) carriers. Violin plot continuous lines indicate median values and dotted lines indicate interquartile range. Significance by ANCOVAs for main effects and post-hoc comparisons controlling for age, sex, and education.

Extended Data Figure 2. BBB breakdown in the hippocampus and parahippocampal gyrus in *APOE4* carriers increases with cognitive domain impairment.

(**a,b**) DCE-MRI BBB permeability, K_{trans} constant, in the hippocampus (HC, **a**) and parahippocampal gyrus (PHG, **b**) in individuals with 0 cognitive domain impaired that are *APOE3* (black, n=70) and *APOE4* (red, n=40) carriers, 1 cognitive domain impaired that are *APOE3* (black, n=18) and *APOE4* (red, n=21) carriers, and 2+ cognitive domains impaired that are *APOE3* (black, n=7) and *APOE4* (red, n=12) carriers. (**c,d**) K_{trans} (estimated marginal means ± SEM from ANCOVA models corrected for age, sex, education, CSF $A\beta_{1-42}$ and pTau status, and HC and PHG volumes) in the HC (**c**) and PHG (**d**) in individuals with 0 cognitive domain impaired that are *APOE3* (black, n=70) and *APOE4* (red, n=40) carriers, 1 cognitive domain impaired that are *APOE3* (black, n=18) and *APOE4* (red, n=21) carriers, and 2+ cognitive domains impaired that are *APOE3* (black, n=7) and *APOE4* (red, n=12) carriers. Panels **a** and **b**: Violin plot continuous lines indicate median values and dotted lines indicate interquartile range. Significance by ANCOVA for main effects and post-hoc comparisons controlling for age, sex, and education. All ANCOVA omnibus tests remained significant at false discovery rate threshold of 0.05.
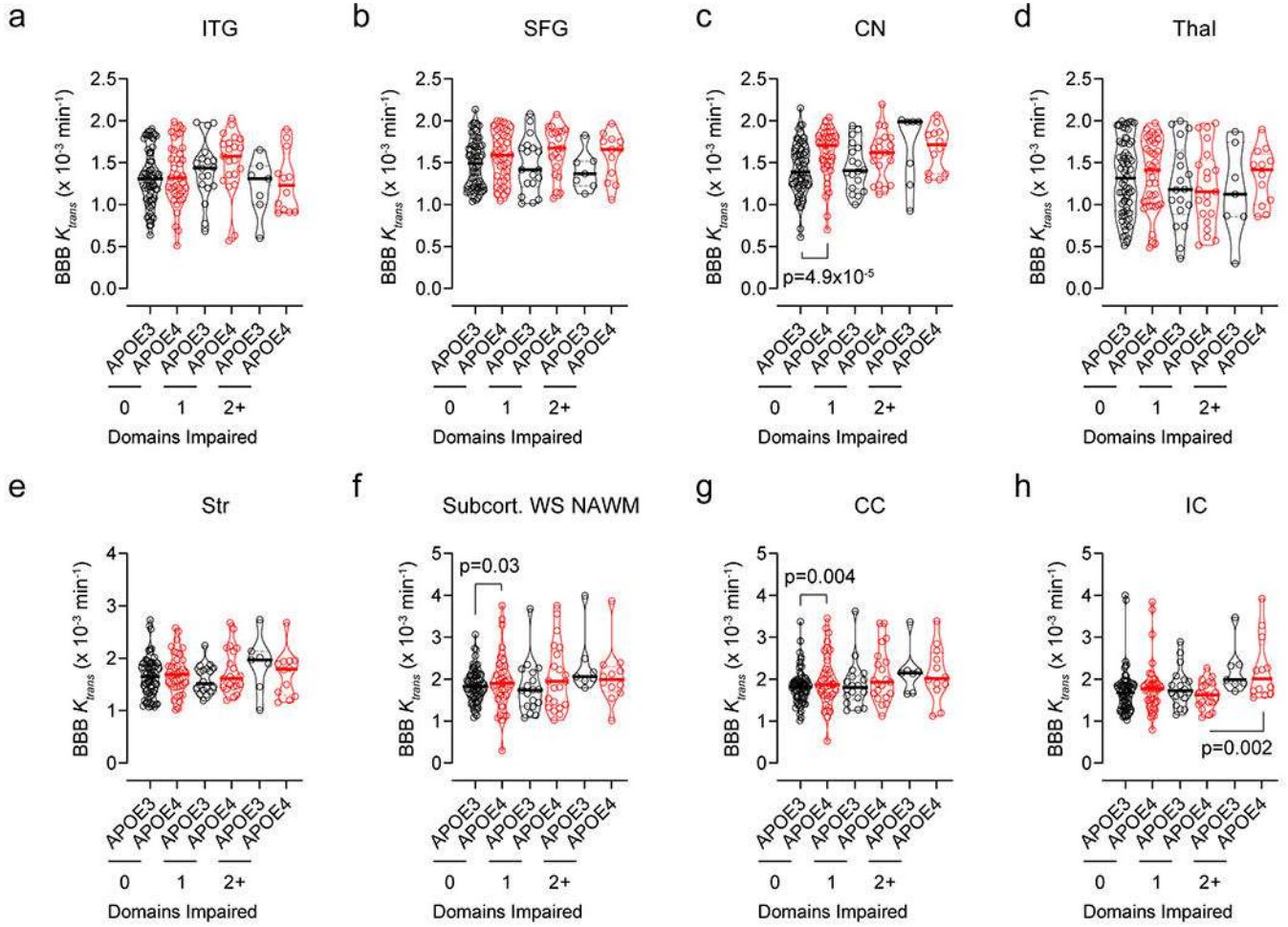
Extended Data Figure 3. Regional BBB K_{trans} constant in eight additional brain regions in *APOE4* carriers and non-carriers (*APOE3*) with different degree of cognitive domain impairment.

DCE-MRI BBB permeability, K_{trans} constant, in the inferior temporal gyrus (ITG, **a**), superior frontal gyrus (SFG, **b**), caudate nucleus (CN, **c**), thalamus (Thal, **d**), striatum (Str, **e**), subcortical watershed normal-appearing white matter (Subcort. WS NAWM, **f**), corpus callosum (CC, **g**), and internal capsule (IC, **h**) in individuals with 0 cognitive domain impaired that are *APOE3* (black, n=70) and *APOE4* (red, n=40) carriers, 1 cognitive domain impaired that are *APOE3* (black, n=18) and *APOE4* (red, n=21) carriers, and 2+ cognitive domains impaired that are *APOE3* (black, n=7) and *APOE4* (red, n=12) carriers. Violin plot continuous lines indicate median values and dotted lines indicate interquartile range. Significance tests from ANCOVAs for main effects and post-hoc comparisons controlling for age, sex, and education.
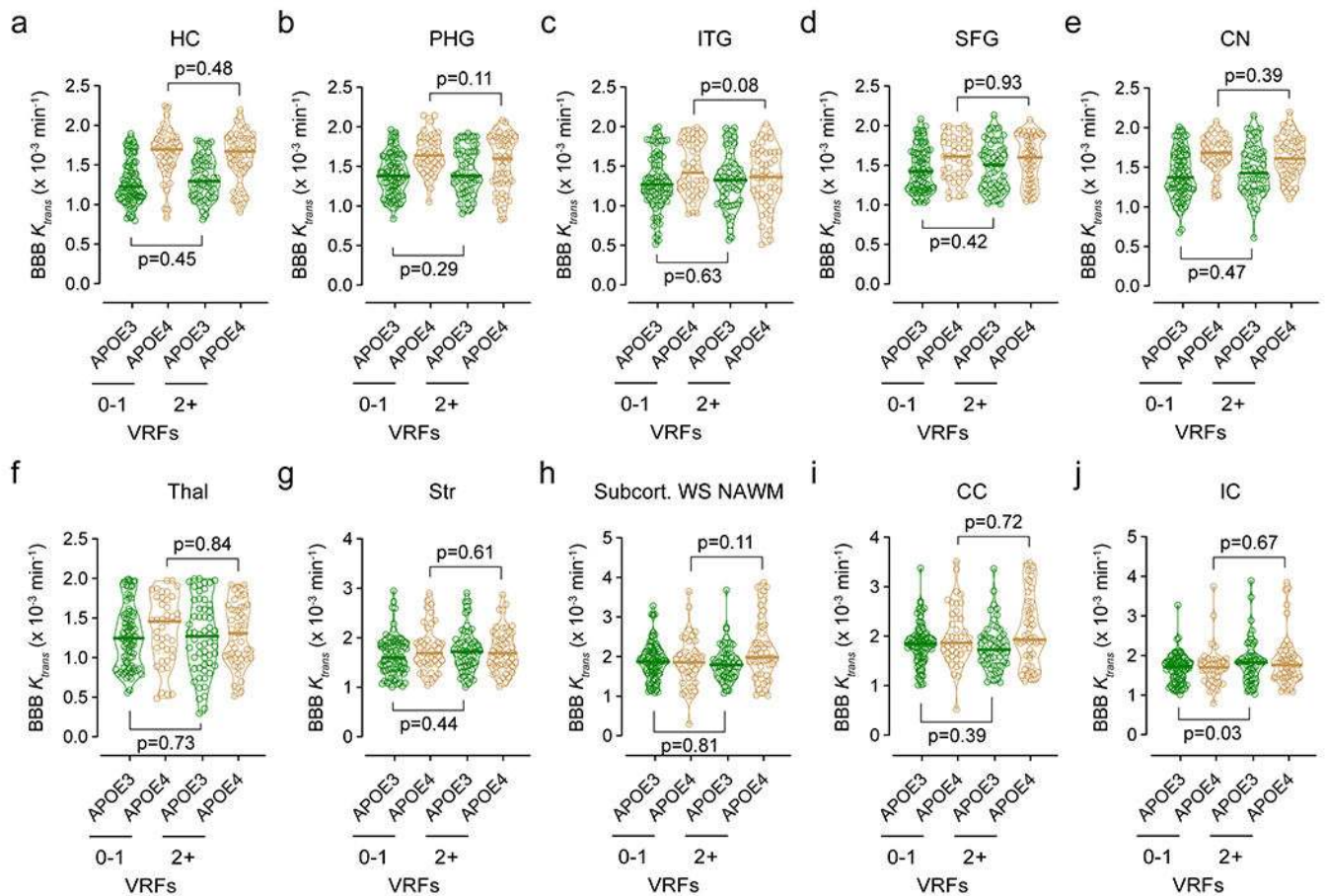
Extended Data Figure 4. Regional BBB K_{trans} constant in all studied brain regions in *APOE4* carriers and non-carriers (*APOE3*) in relation to vascular risk factors.

DCE-MRI BBB permeability, K_{trans} constant, in the hippocampus (HC, **a**), parahippocampal gyrus (PHG, **b**), inferior temporal gyrus (ITG, **c**), superior frontal gyrus (SFG, **d**), caudate nucleus (CN, **e**), thalamus (Thal, **f**), striatum (Str, **g**), subcortical watershed normal-appearing white matter (Subcort. WS NAWM, **h**), corpus callosum (CC, **i**), and internal capsule (IC, **j**) in *APOE3* (black, n=80) and *APOE4* (red, n=42) carriers with 0-1 vascular risk factors (VRFs), and *APOE3* (black, n=58) and *APOE4* (red, n=51) carriers with 2+ VRFs. Violin plot continuous lines indicate median values and dotted lines indicate interquartile range. Significance by ANCOVAs for main effects and post-hoc comparisons controlling for age, sex, and education (ns=non-significant).
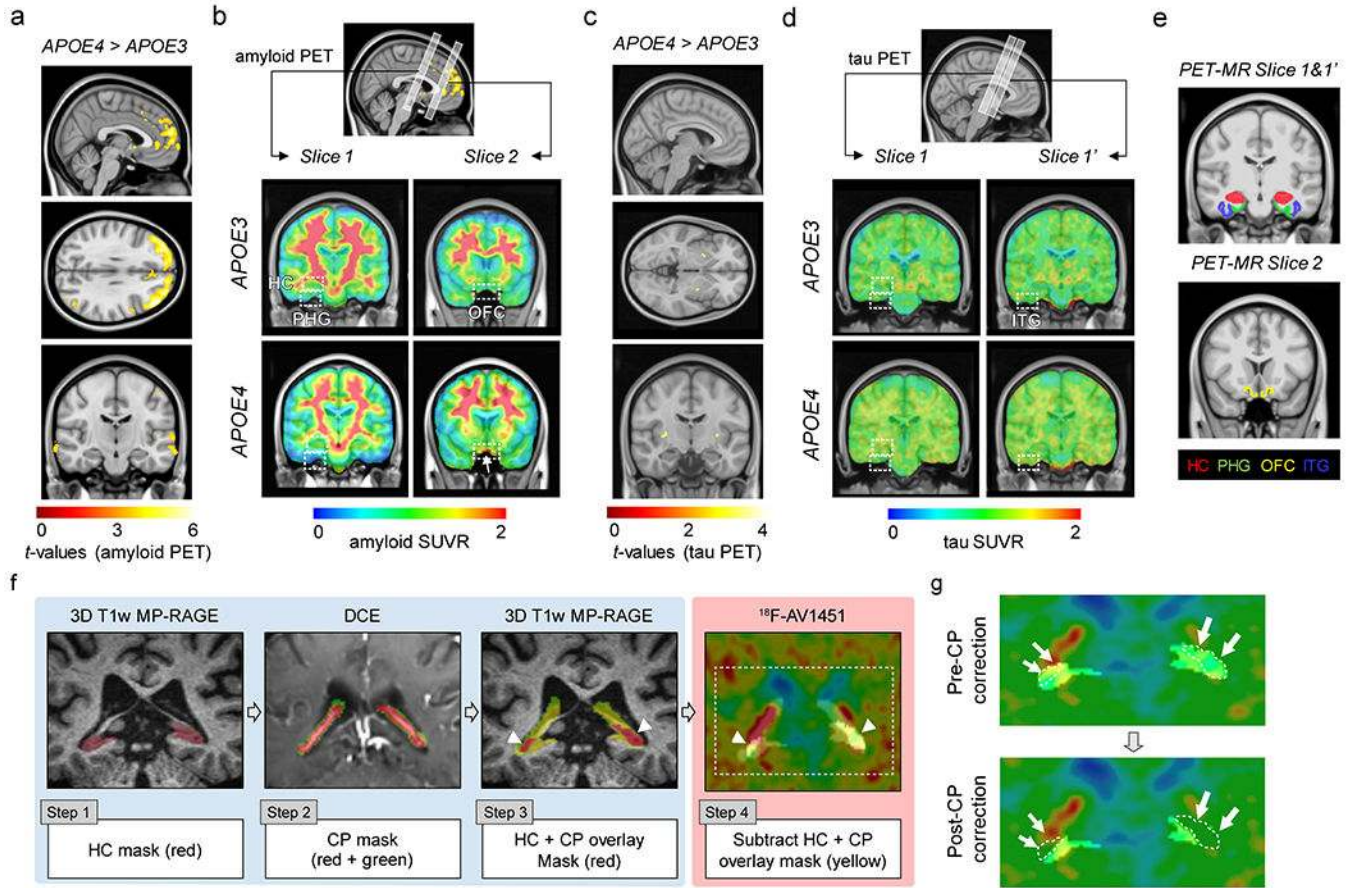
**Extended Data Figure 5. Amyloid and tau PET analysis in *APOE4* carriers and correction of
¹⁸F-AV1451 off-target binding in the choroid plexus.**
All studies were performed in individuals with clinical dementia rating score 0. Amyloid and
tau PET studies were conducted using ^{18}F-Florbetaben (FBB) or ^{18}F-Florbetapir (FBP), and
[18]F-Flortaucipir (AV1451), respectively. For amyloid PET data analysis, FBP and FBB
datasets were combined. (**a**) Uptake of amyloid tracers by the orbital frontal cortex (OFC) in
APOE4 (n=29) relative to *APOE3* (n=45) carriers (voxel-wise 2-sample one-tailed *t*-tests).
(**b**) Representative amyloid PET Standardized Uptake Value Ratios (SUVR) maps from
APOE3 homozygote (*APOE3*) (*upper*) and *APOE4* carrier (*APOE4*) (*lower*). Slices 1 and 2,
regions-of-interest (ROIs) for amyloid PET and BBB DCE-MRI scans (see **e**). Arrow,
amyloid tracer uptake by OFC. The *APOE3* and *APOE4* representative images used FBP. (**c**)
Uptake of tau tracer shows undetectable tau accumulation in *APOE3* (n=60) or *APOE4*
(n=37) carriers (voxel-wise 2-sample one-tailed *t*-tests). (**d**) Representative tau PET SUVR
maps from *APOE3* (*upper*) and *APOE4* (*lower*) carriers. Slice 1 and slice 1', ROIs for tau
PET and BBB DCE-MRI scans (see **e**). (**e**) Coronal 3D scans of regions studied in main
Figure 2: hippocampus (HC; red), parahippocampal gyrus (PHG; green), medial orbital
frontal cortex (OFC; yellow), and inferior temporal gyrus (ITG; blue). (**f**) Correction of [18]F-
AV1451 off-target binding in the choroid plexus: *Step 1*) Hippocampus (HC) masks were
generated from the 3D T1-weighted MP-RAGE; *Step 2*) Choroid plexus (CP) masks were
generated from the T1-weighted VIBE image post-GBCA (flip angle = 15°) image; *Step 3*)

HC and CP masks were overlaid (arrowheads, red); and *Step 4*) CP overlap with HC masks (arrowheads, yellow) were subtracted to obtain CP-corrected HC tau PET signal after adding 6-mm voxel size on top of CP mask generated from DCE data. (**g**) Representative images of HC tau PET signal before (*left*) and after (*right*) applying the CP correction (arrows and white dotted lines = overlap between HC and CP).
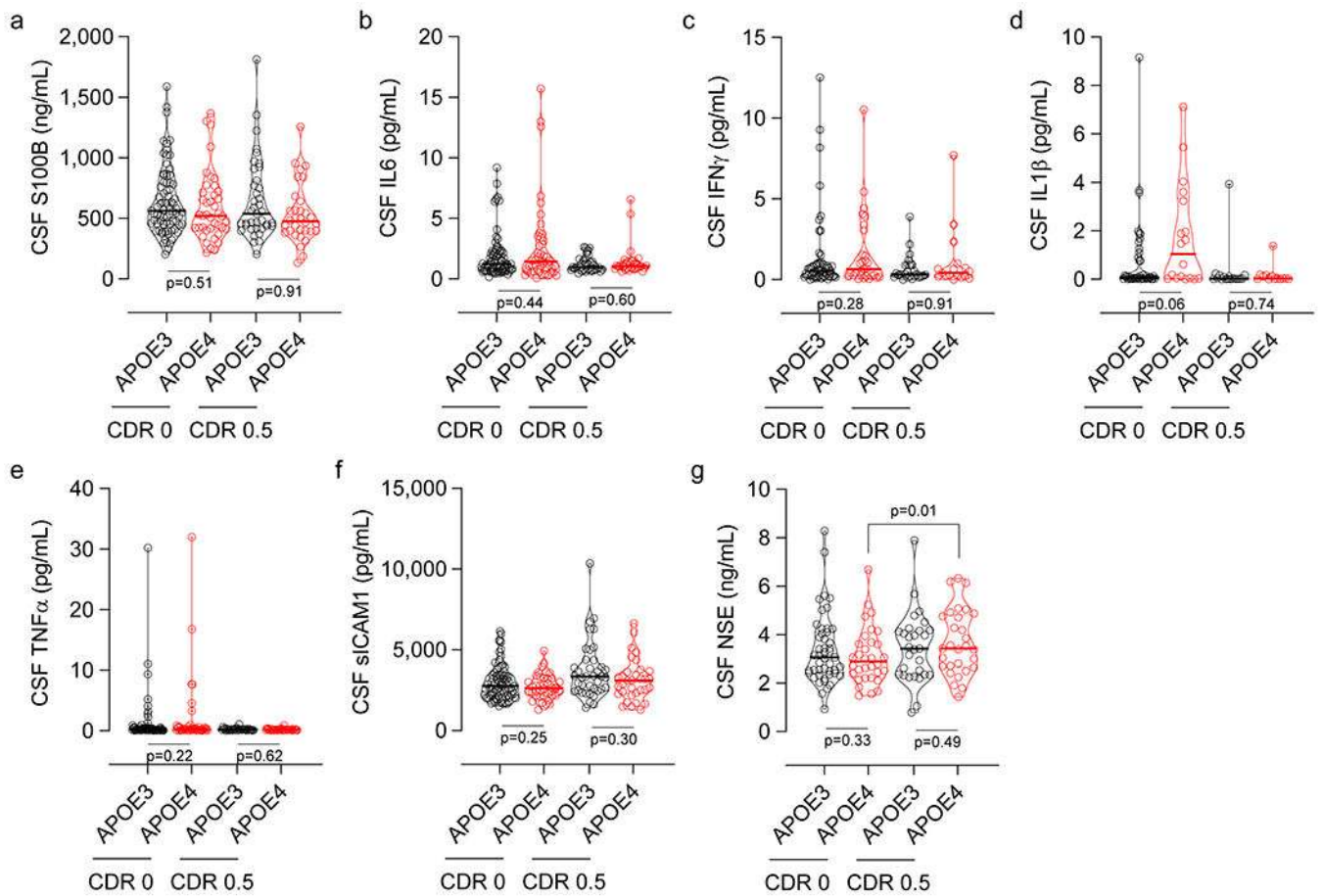
Extended Data Figure 6. CSF biomarkers of glia and inflammatory response and endothelial and neuronal cell injury in *APOE4* carriers and non-carriers (*APOE3*).
(**a**) CSF astrocytic S100 calcium-binding protein B (S100B) levels in CDR 0 *APOE3* (black, n=77) and *APOE4* (red, n=41) carriers, and CDR 0.5 *APOE3* (black, n=39) and *APOE4* (red, n=32) carriers. (**b**) CSF interleukin 6 (IL6) levels in CDR 0 *APOE3* (black, n=71) and *APOE4* (red, n=47) carriers, and CDR 0.5 *APOE3* (black, n=34) and *APOE4* (red, n=32) carriers. (**c**) CSF interferon gamma (IFNγ) levels in CDR 0 *APOE3* (black, n=54) and *APOE4* (red, n=29) carriers, and CDR 0.5 *APOE3* (black, n=25) and *APOE4* (red, n=17) carriers. (**d**) CSF interleukin 1β (IL1β) levels in CDR 0 *APOE3* (black, n=43) and *APOE4* (red, n=18) carriers, and CDR 0.5 *APOE3* (black, n=17) and *APOE4* (red, n=13) carriers. (**e**) CSF tumor necrosis factor α (TNFα) levels in CDR 0 *APOE3* (black, n=70) and *APOE4* (red, n=46) carriers, and CDR 0.5 *APOE3* (black, n=34) and *APOE4* (red, n=32) carriers. (**f**) CSF soluble intercellular adhesion molecule 1 (sICAM1) levels in CDR 0 *APOE3* (black, n=77) and *APOE4* (red, n=40) carriers, and CDR 0.5 *APOE3* (black, n=39) and *APOE4* (red, n=33) carriers. (**g**) CSF Neuron-Specific Enolase (NSE) levels in CDR 0 *APOE3* (black, n=47) and *APOE4* (red, n=32) carriers, and CDR 0.5 *APOE3* (black, n=29) and *APOE4* (red, n=29) carriers. Violin plot continuous lines indicate median values and dotted lines indicate interquartile range. Panels **a** and **b** had one outlier each, which were removed prior to statistical analysis using methods described in Statistical Analyses section.
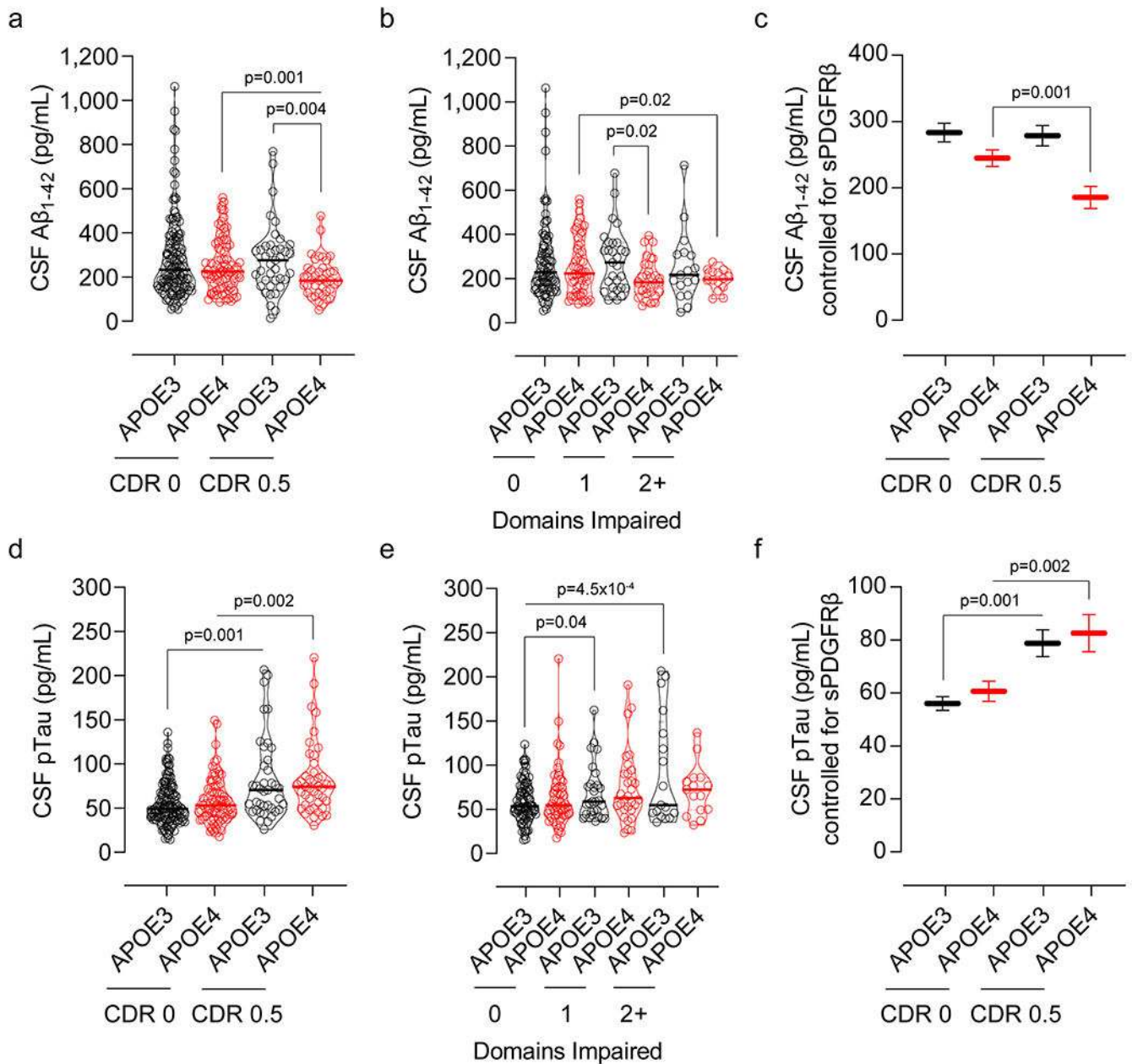
Significance by ANCOVAs for main effects and post-hoc comparisons controlling for age, sex, and education (ns=non-significant).

Extended Data Figure 7. Lower CSF Aβ$_{1-42}$ and increased pTau levels in *APOE4* carriers with cognitive impairment.

(**a**) CSF Aβ$_{1-42}$ levels in CDR 0 *APOE3* (black, n=141) and *APOE4* (red, n=83) and CDR 0.5 *APOE3* (black, n=39) and *APOE4* (red, n=41) carriers. (**b**) CSF Aβ$_{1-42}$ levels in *APOE3* (black, n=89) and *APOE4* (red, n=55) carriers with 0 cognitive domain impaired, *APOE3* (black, n=29) and *APOE4* (red, n=31) carriers with 1 cognitive domain impaired, and *APOE3* (black, n=17) and *APOE4* (red, n=14) carriers with 2+ cognitive domains impaired. (**c**) CSF Aβ$_{1-42}$ levels (estimated marginal means ± SEM from ANCOVA models corrected for age, sex, education, and CSF sPDGFRβ levels) in CDR 0 *APOE3* (black, n=141) and *APOE4* (red, n=83) and CDR 0.5 *APOE3* (black, n=39) and *APOE4* (red, n=41) carriers. (**d**)

CSF pTau levels in CDR 0 *APOE3* (black, n=141) and *APOE4* (red, n=82) and CDR 0.5 *APOE3* (black, n=39) and *APOE4* (red, n=43) carriers. (**e**) CSF pTau levels in *APOE3* (black, n=89) and *APOE4* (red, n=56) carriers with 0 cognitive domain impaired, *APOE3* (black, n=29) and *APOE4* (red, n=30) carriers with 1 cognitive domain impaired, and *APOE3* (black, n=17) and *APOE4* (red, n=15) carriers with 2+ cognitive domains impaired. (**f**) CSF pTau levels (estimated marginal means ± SEM from ANCOVA models corrected for age, sex, education, and CSF sPDGFRβ levels) in CDR 0 *APOE3* (black, n=141) and *APOE4* (red, n=82) and CDR 0.5 *APOE3* (black, n=39) and *APOE4* (red, n=43) carriers. Violin plot continuous lines indicate median values and dotted lines indicate interquartile range. CSF Aβ$_{1-42}$ and pTau values were log10-transformed due to non-normal distribution prior to statistical analysis. Significance tests from ANCOVAs for main effects and post-hoc comparisons controlling for age, sex, and education.
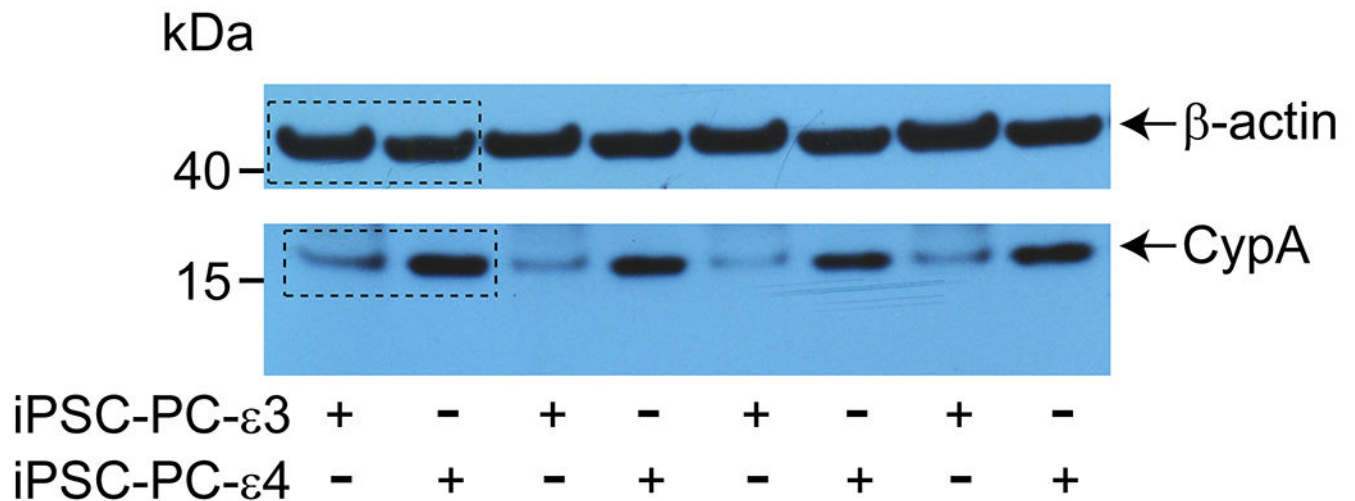
Extended Data Figure 8. Full scans of western blots.
Full scans of western blots for CypA shown in Figure 4 panel m (top).

Extended Data Table 1.

APOE3 and *APOE4* participants studied for regional blood-brain barrier permeability changes by dynamic contrast-enhanced magnetic resonance imaging (DCE-MRI).

APOE Genotype	APOE3	APOE4	APOE3	APOE4
Clinical Dementia Rating (CDR)	0	0	0.5	0.5
No. of participants	130	76	14	25
Age at MRI, years, Mean (SD)	69.9 (7.9)	67.3 (8.7)	73.8 (8.3)	69.4 (8.7)
Female, %	62.3	57.9	42.9	56
Education, years, Mean (SD)	16.6 (2.7)	16.7 (2.0)	16.4 (2.5)	17.1 (2.1)
Cognitive domain impairment, No. 0,1, 2+	78, 17, 2	38, 16,4	6, 2,6	6, 8,9
Vascular risk factors, No. 0-1, 2+	77, 53	38, 38	8,6	10, 15

Extended Data Table 2

a. *APOE3* and *APOE4* participants studied for regional amyloid brain accumulation by PET and blood-brain barrier permeability changes by DCE-MRI. FBB, participants who received ^{18}F-Florbetaben; FBP, participants who received ^{18}F-Florbetapir.

b. *APOE3* and *APOE4* participants studied for regional tau brain accumulation by PET and blood-brain barrier permeability changes by DCE-MRI.

APOE Genotype	APOE3	APOE4
Clinical Dementia Rating (CDR)	0	0
No. of participants	45	29
No. of participants (FBB, FBP)	5, 40	9, 20
Age at amyloid PET, years, Mean (SD)	68.4 (7.5)	65.7 (8.8)

APOE Genotype	APOE3	APOE4
Female, %	73.3	65.5
Education, years, Mean (SD)	16.7 (2.7)	16.5 (2.1)
Cognitive domain impairment, No. 0,1, 2+	24, 4, 0	17, 4, 1
Vascular risk factors, No. 0-1, 2+	23, 22	19, 10
APOE Genotype	APOE3	APOE4
Clinical Dementia Rating (CDR)	0	0
No. of participants	60	37
Age at tau PET, years, Mean (SD)	68.7 (7.9)	64.0 (8.4)
Female, %	66.6	37.8
Education, years, Mean (SD)	16.5 (2.7)	16.6 (2.1)
Cognitive domain impairment, No. 0,1, 2+	27, 5, 1	15, 6, 1
Vascular risk factors, No. 0-1, 2+	36, 24	23, 14

Extended Data Table 3.

APOE3 and *APOE4* participants studied for CSF sPDGFRβ levels.

APOE Genotype	APOE3	APOE4	APOE3	APOE4
Clinical Dementia Rating (CDR)	0	0	0.5	0.5
No. of participants	157	105	40	48
Age at LP, years, Mean (SD)	70.2 (8.9)	67.3 (9.9)	76.5 (7.3)	72.8 (8.1)
Female, %	64	61	39	37
Education, years, Mean (SD)	16.5 (2.7)	16.3 (2.3)	15.7 (2.8)	16.2 (2.8)
Cognitive domain impairment, No. 0,1, 2+	91,20,2	62, 17,2	9, 8, 14	12, 16, 15
Vascular risk factors, No. 0-1, 2+	100, 57	57, 48	22, 18	18, 30

Supplementary Material

Refer to Web version on PubMed Central for supplementary material.

Acknowledgments

References

1. Wardlaw JM et al. Neuroimaging standards for research into small vessel disease and its contribution to ageing and neurodegeneration. Lancet Neurol. 12, 822–838 (2013). [PubMed: 23867200]

2. Kapasi A, DeCarli C & Schneider JA Impact of multiple pathologies on the threshold for clinically overt dementia. Acta Neuropathol. (Berl.) 134, 171–186 (2017). [PubMed: 28488154]

3. Iadecola C The Neurovascular Unit Coming of Age: A Journey through Neurovascular Coupling in Health and Disease. Neuron 96, 17–42 (2017). [PubMed: 28957666]

4. Iturria-Medina Y et al. Early role of vascular dysregulation on late-onset Alzheimer's disease based on multifactorial data-driven analysis. Nat. Commun 7, 11934 (2016). [PubMed: 27327500]

5. Sweeney MD, Sagare AP & Zlokovic BV Blood-brain barrier breakdown in Alzheimer disease and other neurodegenerative disorders. Nat. Rev. Neurol 14, 133–150 (2018). [PubMed: 29377008]

6. Sweeney MD et al. Vascular dysfunction-The disregarded partner of Alzheimer's disease. Alzheimers Dement. J. Alzheimers Assoc 15, 158–167 (2019).

7. Nation DA et al. Blood-brain barrier breakdown is an early biomarker of human cognitive dysfunction. Nat. Med 25, 270–276 (2019). [PubMed: 30643288]

8. Montagne A et al. Blood-brain barrier breakdown in the aging human hippocampus. Neuron 85, 296–302 (2015). [PubMed: 25611508]

9. van de Haar HJ et al. Neurovascular unit impairment in early Alzheimer's disease measured with magnetic resonance imaging. Neurobiol. Aging 45, 190–196 (2016). [PubMed: 27459939]

10. van de Haar HJ et al. Blood-Brain Barrier Leakage in Patients with Early Alzheimer Disease. Radiology 281, 527–535 (2016). [PubMed: 27243267]

11. Corder EH et al. Gene dose of apolipoprotein E type 4 allele and the risk of Alzheimer's disease in late onset families. Science 261, 921–923 (1993). [PubMed: 8346443]

12. Roses AD Apolipoprotein E alleles as risk factors in Alzheimer's disease. Annu. Rev. Med 47, 387–400 (1996). [PubMed: 8712790]

13. Farrer LA et al. Effects of age, sex, and ethnicity on the association between apolipoprotein E genotype and Alzheimer disease. A meta-analysis. APOE and Alzheimer Disease Meta Analysis Consortium. JAMA 278, 1349–1356 (1997). [PubMed: 9343467]

14. Genin E et al. APOE and Alzheimer disease: a major gene with semi-dominant inheritance. Mol. Psychiatry 16, 903–907 (2011). [PubMed: 21556001]

15. Hultman K, Strickland S & Norris EH The APOE ε4/ε4 genotype potentiates vascular fibrin(ogen) deposition in amyloid-laden vessels in the brains of Alzheimer's disease patients. J. Cereb. Blood Flow Metab. Off. J. Int. Soc. Cereb. Blood Flow Metab 33, 1251–1258 (2013).

16. Halliday MR et al. Accelerated pericyte degeneration and blood-brain barrier breakdown in apolipoprotein E4 carriers with Alzheimer's disease. J. Cereb. Blood Flow Metab. Off. J. Int. Soc. Cereb. Blood Flow Metab 36, 216–227 (2016).

17. Salloway S et al. Effect of APOE genotype on microvascular basement membrane in Alzheimer's disease. J. Neurol. Sci 203–204, 183–187 (2002).

18. Zipser BD Microvascular injury and blood-brain barrier leakage in Alzheimer/'s disease. Neurobiol Aging 28, 977–986 (2007). [PubMed: 16782234]

19. Bell RD et al. Apolipoprotein E controls cerebrovascular integrity via cyclophilin A. Nature 485, 512–516 (2012). [PubMed: 22622580]

20. Armulik A et al. Pericytes regulate the blood-brain barrier. Nature 468, 557–561 (2010). [PubMed: 20944627]

21. Bell RD et al. Pericytes control key neurovascular functions and neuronal phenotype in the adult brain and during brain aging. Neuron 68, 409–427 (2010). [PubMed: 21040844]

22. Nikolakopoulou AM et al. Pericyte loss leads to circulatory failure and pleiotrophin depletion causing neuron loss. Nat. Neurosci 22, 1089–1098 (2019). [PubMed: 31235908]

23. Jack CR et al. NIA-AA Research Framework: Toward a biological definition of Alzheimer's disease. Alzheimers Dement. J. Alzheimers Assoc 14, 535–562 (2018).

24. Pan C et al. Diagnostic Values of Cerebrospinal Fluid T-Tau and Aβ_{42} using Meso Scale Discovery Assays for Alzheimer's Disease. J. Alzheimers Dis. JAD 45, 709–719 (2015). [PubMed: 25613100]

25. Roe CM et al. Amyloid imaging and CSF biomarkers in predicting cognitive impairment up to 7.5 years later. Neurology 80, 1784–1791 (2013). [PubMed: 23576620]

26. Montagne A, Zhao Z & Zlokovic BV Alzheimer's disease: A matter of blood-brain barrier dysfunction? J. Exp. Med 214, 3151–3169 (2017). [PubMed: 29061693]

27. Bennett RE et al. Tau induces blood vessel abnormalities and angiogenesis-related gene expression in P301L transgenic mice and human Alzheimer's disease. Proc. Natl. Acad. Sci. U. S. A 115, E1289–E1298 (2018). [PubMed: 29358399]

28. Fouquet M, Besson FL, Gonneaud J, La Joie R & Chételat G Imaging brain effects of APOE4 in cognitively normal individuals across the lifespan. Neuropsychol. Rev 24, 290–299 (2014). [PubMed: 25146994]

29. Schultz SA et al. Widespread distribution of tauopathy in preclinical Alzheimer's disease. Neurobiol. Aging 72, 177–185 (2018). [PubMed: 30292840]

30. Miners JS, Kehoe PG, Love S, Zetterberg H & Blennow K CSF evidence of pericyte damage in Alzheimer's disease is associated with markers of blood-brain barrier dysfunction and disease pathology. Alzheimers Res. Ther 11, 81 (2019). [PubMed: 31521199]

31. Stanciu C, Trifan A, Muzica C & Sfarti C Efficacy and safety of alisporivir for the treatment of hepatitis C infection. Expert Opin. Pharmacother 20, 379–384 (2019). [PubMed: 30576256]

32. Morris JC et al. The Uniform Data Set (UDS): clinical and cognitive variables and descriptive data from Alzheimer Disease Centers. Alzheimer Dis. Assoc. Disord 20, 210–216 (2006). [PubMed: 17132964]

33. Morris JC The Clinical Dementia Rating (CDR): current version and scoring rules. Neurology 43, 2412–2414 (1993).

34. Nation DA et al. Antemortem pulse pressure elevation predicts cerebrovascular disease in autopsy-confirmed Alzheimer's disease. J. Alzheimers Dis. JAD 30, 595–603 (2012). [PubMed: 22451309]

35. Bangen KJ et al. Aggregate effects of vascular risk factors on cerebrovascular changes in autopsy-confirmed Alzheimer's disease. Alzheimers Dement. J. Alzheimers Assoc 11, 394–403.e1 (2015).

36. Jak AJ et al. Quantification of five neuropsychological approaches to defining mild cognitive impairment. Am. J. Geriatr. Psychiatry Off. J. Am. Assoc. Geriatr. Psychiatry 17, 368–375 (2009).

37. Jak AJ et al. Neuropsychological Criteria for Mild Cognitive Impairment and Dementia Risk in the Framingham Heart Study. J. Int. Neuropsychol. Soc. JINS 22, 937–943 (2016). [PubMed: 27029348]

38. Weintraub S et al. The Alzheimer's Disease Centers' Uniform Data Set (UDS): the neuropsychologic test battery. Alzheimer Dis. Assoc. Disord 23, 91–101 (2009). [PubMed: 19474567]

39. Besser L et al. Version 3 of the National Alzheimer's Coordinating Center's Uniform Data Set. Alzheimer Dis. Assoc. Disord 32, 351–358 (2018). [PubMed: 30376508]

40. Delis D, Kramer J, Kaplan E & Ober B California Verbal Learning Test. (PsychCorp, 2000).

41. Montagne A et al. Undetectable gadolinium brain retention in individuals with an age-dependent blood-brain barrier breakdown in the hippocampus and mild cognitive impairment. Alzheimers Dement. J. Alzheimers Assoc 15, 1568–1575 (2019).

42. Fischl B FreeSurfer. NeuroImage 62, 774–781 (2012). [PubMed: 22248573]

43. Fischl B et al. Whole brain segmentation: automated labeling of neuroanatomical structures in the human brain. Neuron 33, 341–355 (2002). [PubMed: 11832223]

44. Desikan RS et al. An automated labeling system for subdividing the human cerebral cortex on MRI scans into gyral based regions of interest. NeuroImage 31, 968–980 (2006). [PubMed: 16530430]

45. Fischl B & Dale AM Measuring the thickness of the human cerebral cortex from magnetic resonance images. Proc. Natl. Acad. Sci. U. S. A 97, 11050–11055 (2000). [PubMed: 10984517]

46. Fischl B, Sereno MI, Tootell RB & Dale AM High-resolution intersubject averaging and a coordinate system for the cortical surface. Hum. Brain Mapp 8, 272–284 (1999). [PubMed: 10619420]

47. Dinov I et al. Neuroimaging study designs, computational analyses and data provenance using the LONI pipeline. PloS One 5, (2010).

48. Sepehrband F et al. Neuroanatomical morphometric characterization of sex differences in youth using statistical learning. NeuroImage 172, 217–227 (2018). [PubMed: 29414494]

49. Cabeen RP, Laidlaw DH & Toga AW Quantitative imaging toolkit: Software for interactive 3D visualization, data exploration, and computational analysis of neuroimaging datasets. in Proceedings of the International Society for Magnetic Resonance in Medicine (ISMRM) vol. 2854 (2018).

50. Jenkinson M, Bannister P, Brady M & Smith S Improved optimization for the robust and accurate linear registration and motion correction of brain images. NeuroImage 17, 825–841 (2002). [PubMed: 12377157]

51. Bullich S et al. Optimal Reference Region to Measure Longitudinal Amyloid-β Change with 18F-Florbetaben PET. J. Nucl. Med. Off. Publ. Soc. Nucl. Med 58, 1300–1306 (2017).

52. Marquié M et al. Lessons learned about [F-18]-AV-1451 off-target binding from an autopsy-confirmed Parkinson's case. Acta Neuropathol. Commun 5, 75 (2017). [PubMed: 29047416]

53. Mishra S et al. AV-1451 PET imaging of tau pathology in preclinical Alzheimer disease: Defining a summary measure. NeuroImage 161, 171–178 (2017). [PubMed: 28756238]

54. TCW J et al. Cholesterol and matrisome pathways dysregulated in human ɛ4 glia. bioRxiv (2019) doi:10.1101/713362.

55. Faal T et al. Induction of Mesoderm and Neural Crest-Derived Pericytes from Human Pluripotent Stem Cells to Study Blood-Brain Barrier Interactions. Stem Cell Rep. 12, 451–460 (2019).

56. Aggarwal CC Outlier analysis. (Springer, 2013).

57. Sagare AP, Sweeney MD, Makshanoff J & Zlokovic BV Shedding of soluble platelet-derived growth factor receptor-β from human brain pericytes. Neurosci. Lett 607, 97–101 (2015). [PubMed: 26407747]

58. Glickman ME, Rao SR & Schultz MR False discovery rate control is a recommended alternative to Bonferroni-type adjustments in health studies. J. Clin. Epidemiol 67, 850–857 (2014). [PubMed: 24831050]
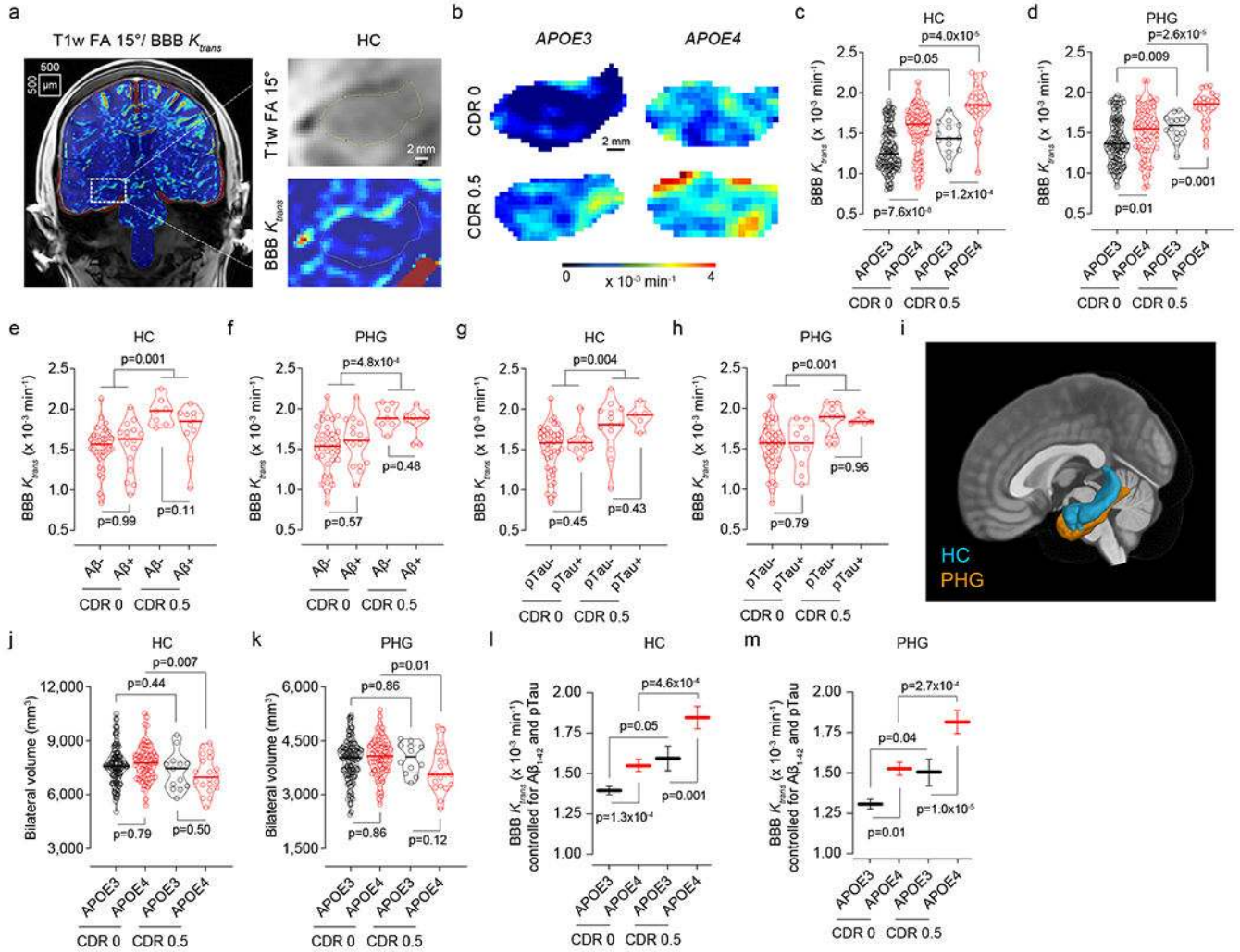
Figure 1. Blood-brain barrier breakdown in the hippocampus and parahippocampal gyrus in *APOE4* carriers increases with cognitive impairment independently of CSF Aβ and tau status.
(**a**,**b**) Blood-brain barrier (BBB) permeability K_{trans} maps generated by dynamic contrast-enhanced magnetic resonance imaging in the hippocampus (HC) of *APOE3* homozygotes (*APOE3*) and *APOE4* carriers (*APOE4*) with clinical dementia rating (CDR) score 0 or 0.5. (**c**,**d**) BBB permeability, K_{trans} constant, in the HC (**c**) and parahippocampal gyrus (PHG, **d**) in CDR 0 *APOE3* (black, n=128) and *APOE4* (red, n=68) and CDR 0.5 *APOE3* (black, n=14) and *APOE4* (red, n=25) carriers. (**e**,**f**) K_{trans} values in the HC (**e**) and PHG (**f**) in *APOE4* carriers CDR 0 Aβ$_{1-42}$ negative (Aβ-; n=37) or positive (Aβ+; n=16), and CDR 0.5 Aβ- (n=7) or Aβ+ (n=10). (**g**,**h**) K_{trans} values in the HC (**g**) and PHG (**h**) in *APOE4* carriers CDR 0 pTau negative (pTau−; n=42) or positive (pTau+; n=10), and CDR 0.5 pTau− (n=13) or pTau+ (n=5). (**i**) HC (blue) and PHG (orange) overlaid on a 3D template. (**j**,**k**) HC (**j**) and PHG (**k**) volumes in CDR 0 *APOE3* (n=124) and *APOE4* (n=75) and CDR 0.5 *APOE3* (n=13) and *APOE4* (n=20) carriers. (**l**,**m**) K_{trans} (estimated marginal means ± SEM from ANCOVA models corrected for age, sex, education, CSF Aβ$_{1-42}$ and pTau status, and HC and PHG volumes) in the HC (**l**) and PHG (**m**) in CDR 0 *APOE3* (black, HC n=125; PHG n=128) and *APOE4* (red, HC and PHG n=68) and CDR 0.5 *APOE3* (black, HC n=12; PHG

n=14) and *APOE4* (red, HC n=20; PHG n=25) carriers. In **c-h**, **j**, and **k**, continuous line indicates median value; dotted line indicates interquartile range. Significance by ANCOVA for main effects and post-hoc comparisons controlling for age, sex, and education. All ANCOVA omnibus tests remained significant at false discovery rate threshold of 0.05.
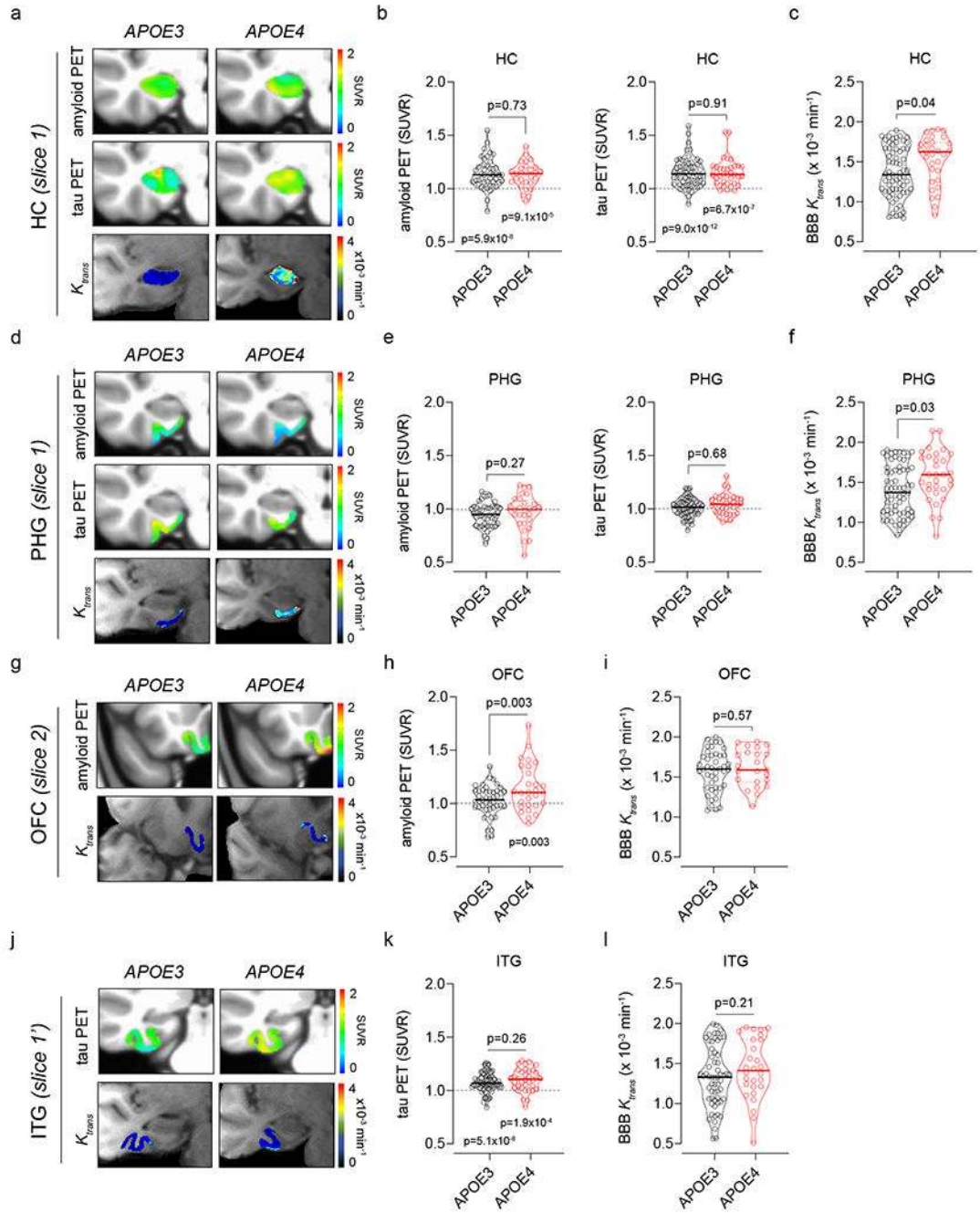
Figure 2. Blood-brain barrier breakdown in *APOE4* carriers is independent of amyloid and tau brain accumulation.

All studies were performed in individuals with clinical dementia rating score 0. (**a**) Representative superimposed left-hippocampus (HC) amyloid PET (*top*), tau PET (*middle*), and BBB K_{trans} maps (*bottom*) from *APOE3* (*left*) and *APOE4* (*right*) carriers. (**b,c**) HC: amyloid and tau tracer uptake (**b**) and BBB K_{trans} constant (**c**) in *APOE3* (n=45, 60, and 65) and *APOE4* (n=29, 37, and 31) carriers. (**d**) Representative superimposed left-parahippocampal gyrus (PHG) amyloid PET (*top*), tau PET (*middle*), and BBB K_{trans} maps

(*bottom*) from *APOE3* (*left*) and *APOE4* (*right*) carriers. (**e,f**) PHG: amyloid and tau tracer uptake (**e**) and BBB K_{trans} constant (**f**) in *APOE3* (n=45, 60, and 65) and *APOE4* (n=29, 37, and 31) carriers. (**g**) Representative superimposed left-medial orbital frontal cortex (OFC) amyloid PET (*top*) and BBB K_{trans} maps (*bottom*) from *APOE3* (*left*) and *APOE4* (*right*) carriers. (**h,i**) OFC: amyloid tracer uptake (**h**) and BBB K_{trans} constant (**i**) in *APOE3* (n=45 and 44) and *APOE4* (n=29 and 23) carriers. (**j**) Representative superimposed left-inferior temporal gyrus (ITG) tau PET (*top*) and BBB K_{trans} maps (*bottom*) from *APOE3* (*left*) and *APOE4* (*right*) carriers. (**k,l**) ITG: tau tracer uptake (**l**) and BBB K_{trans} constant (**l**) in *APOE3* (n=60 and 59) and *APOE4* (n=37 and 28) carriers. In **b**, **c**, **e**, **f**, **h**, **i**, **k**, and **l**, continuous lines indicate median values and dotted lines indicate interquartile range. The BBB K_{trans} constant was determined in all participants (see Extended Data Tables 2a,b) who received either both amyloid and tau tracers (n=58), only amyloid tracer (n=9) or only tau tracer (n= 29). Significance by ANCOVA for group comparisons controlling for age, sex, and education, and one-tailed *t*-tests for comparison of PET values to SUVR = 1.
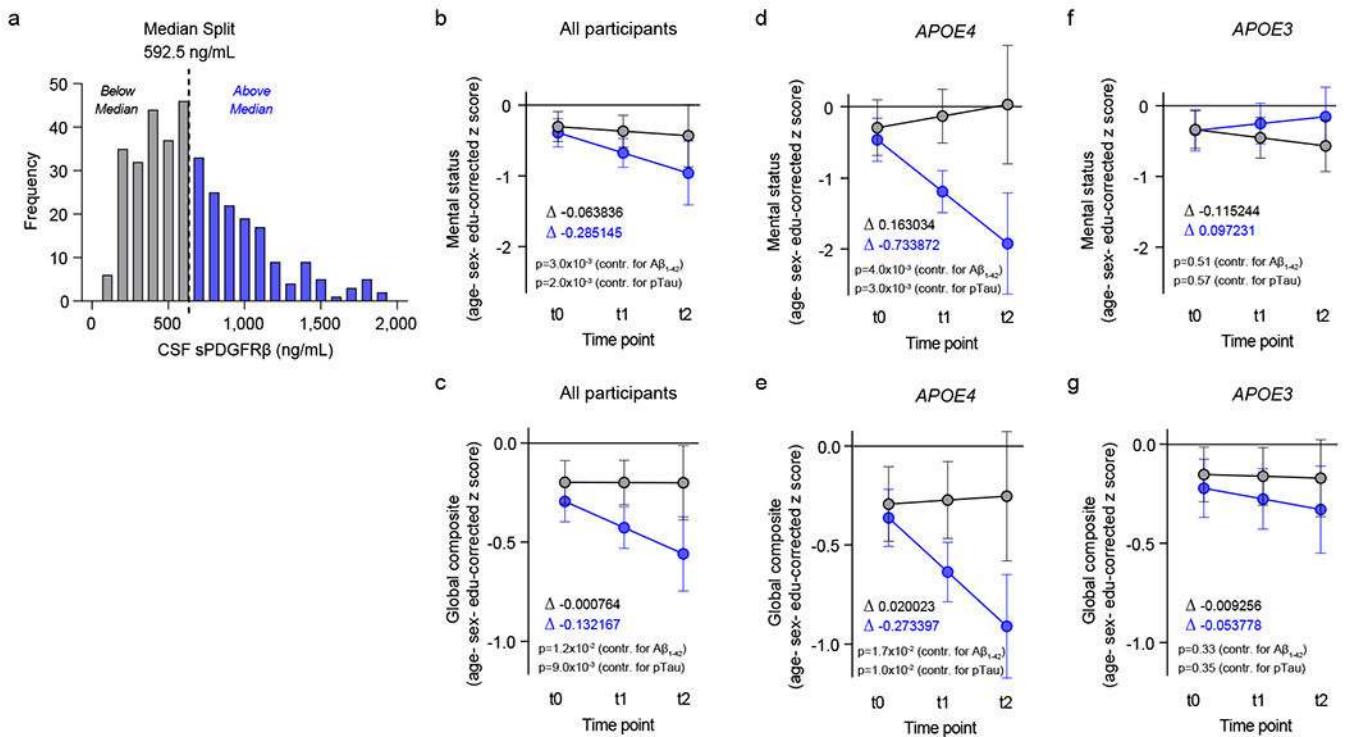
Figure 3. Elevated baseline CSF levels of pericyte injury biomarker sPDGFRβ predict cognitive decline in *APOE4* carriers.

(**a**) Histogram frequency distribution of CSF sPDGFRβ values using median split to divide participants into two groups with high (*blue*, above median 600-2,000 ng/ml) and low (*grey*, below median; 0-600 ng/ml) baseline CSF sPDGFRβ levels. All longitudinal analyses used baseline CSF sPDGFRβ as a continuous predictor of future cognitive decline. (**b-c**) Linear mixed model analysis of all studied participants (n=146) followed over 2-year intervals for up to 4.5 years after baseline lumbar puncture (LP) shows that higher baseline CSF sPDGFRβ (*blue*) predicts greater decline in demographically-corrected mental status exam scores over time (p=0.01), which remains significant after controlling for CSF Aβ (p=0.002) and pTau (p=0.002) status (**b**), and in global cognitive composite scores (p=0.01), which also remains significant after controlling for CSF Aβ (p=0.017) and pTau (p=0.01) status (**c**). (**d-e**) Higher CSF sPDGFRβ (*blue*) in *APOE4* carriers (n=58) predicts future decline in mental status exam scores (p=0.005) after controlling for CSF Aβ (p=0.004) and pTau (p=0.003) status (**d**), and in global cognitive composite scores (p=0.02) after controlling for CSF Aβ (p=0.02) and pTau (p=0.01) status (**e**). (**f-g**) Baseline CSF sPDGFRβ does not predict decline in *APOE3* homozygotes (n=88) on either mental status (**f**) or global composite (**g**) scores regardless of CSF Aβ or pTau status. Panels **b-g**, for graphical depiction, separate lines indicate median split of baseline CSF sPDGFRβ (*grey*, below median; *blue*, above median). Δ slopes provided for median split of baseline CSF sPDGFRβ groups (*grey*, below median; *blue*, above median). Time was modeled as $t_0 = -1$ to 0.5 years post-LP, $t_1 = 0.5$ to 2.5 years post-LP, and $t_2 = 2.5$ to 4.5 years post-LP. The error bars are SE of the estimate. In panels **b-g**, significance by linear mixed model analysis; no multiple comparison correction applied. See Supplementary Information Tables 2–4 for detailed statistics.
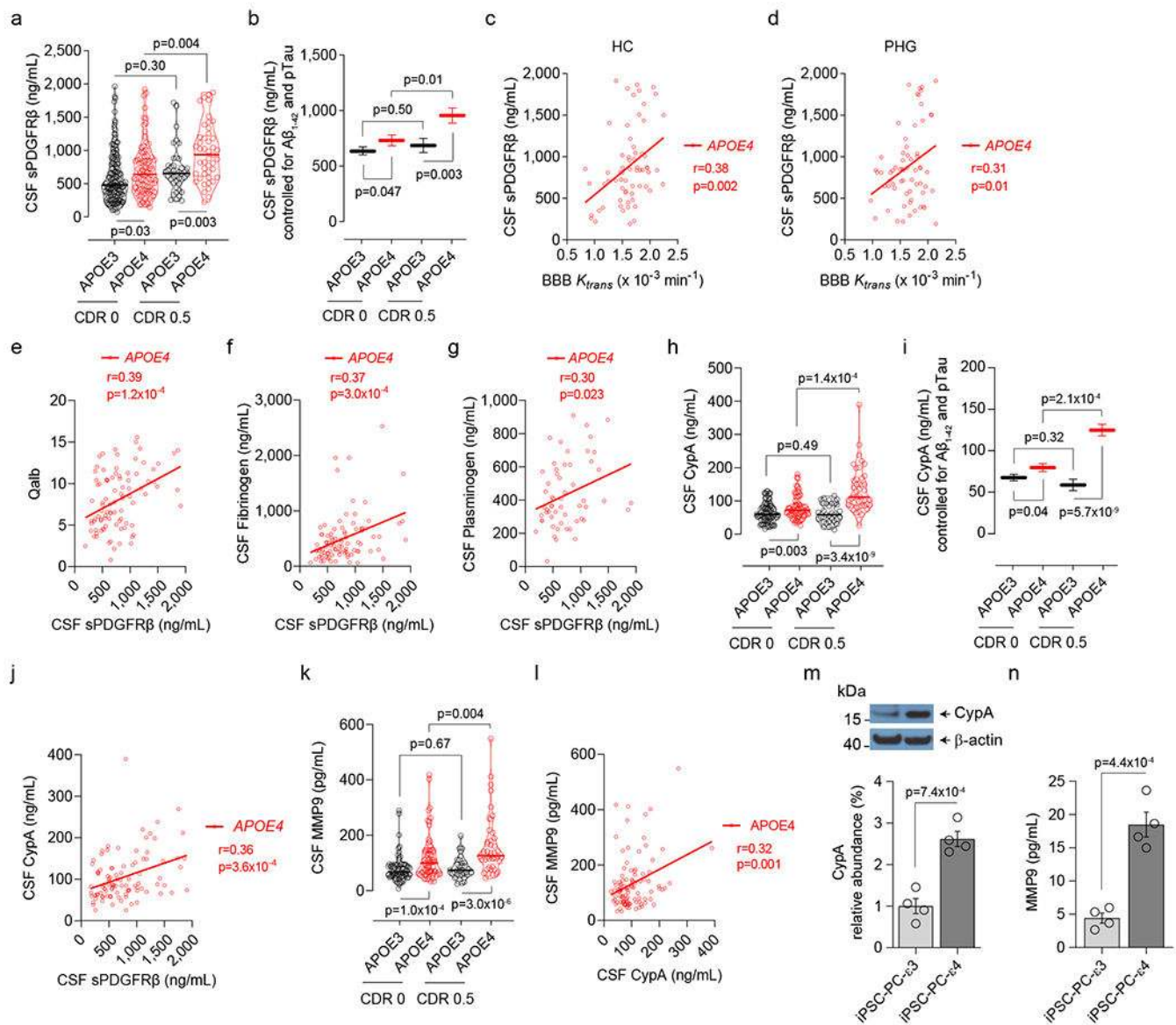
Figure 4. Elevated CSF sPDGFRβ, cyclophilin A and matrix metalloproteinase-9 in *APOE4* carriers.

(**a**) CSF sPDGFRβ in CDR 0 *APOE3* (black, n=152) and *APOE4* (red, n=95) and CDR 0.5 *APOE3* (black, n=42) and *APOE4* (red, n=45) carriers. (**b**) CSF sPDGFRβ (estimated marginal means ± SEM from ANCOVA models corrected for age, sex, education, CSF Aβ$_{1-42}$ and pTau status) in CDR 0 *APOE3* (black, n=152) and *APOE4* (red, n=95) and CDR 0.5 *APOE3* (black, n=42) and *APOE4* (red, n=45) carriers. (**c,d**) CSF sPDGFRβ and BBB K_{trans} correlation in the hippocampus (HC, n=65; **c**) and parahippocampal gyrus (PHG, n=65; **d**) in *APOE4* carriers. (**e-g**) Correlations between CSF sPDGFRβ and albumin quotient (Qalb, n=92; **e**), fibrinogen (n=93; **f**), and plasminogen (n=57; **g**) in *APOE4* carriers. (**h**) CSF cyclophilin A (CypA) in CDR 0 *APOE3* (black, n=75) and *APOE4* (red, n=62) and CDR 0.5 *APOE3* (black, n=33) and *APOE4* (red, n=45) carriers. (**i**) CSF CypA (estimated marginal means ± SEM from ANCOVA models corrected for age, sex, education,

CSF Aβ_{1-42} and pTau status) in CDR 0 *APOE3* (black, n=75) and *APOE4* (red, n=62) and CDR 0.5 *APOE3* (black, n=33) and *APOE4* (red, n=45) carriers. (**j**) CSF CypA and sPDGFRβ correlation in *APOE4* carriers (n=96). (**k**) CSF matrix metalloproteinase-9 (MMP9) in CDR 0 *APOE3* (black, n=72) and *APOE4* (red, n=68) and CDR 0.5 *APOE3* (black, n=33) and *APOE4* (red, n=45) carriers. (**l**) CSF MMP9 and CypA correlation in *APOE4* carriers (n=104). (**m,n**) CypA (**m**; see Extended Data Fig. 8), and secreted MMP9 in the culture medium (**n**), in human iPSC-derived *APOE3* (ε3/ε3) and *APOE4* (ε4/ε4) pericytes. Mean + SEM from four independent culture replicates. In **a, h** and **k**, continuous lines indicate median values and dotted lines interquartile range. Significance by ANCOVA for main effects and post-hoc comparisons controlling for age, sex, and education. Panels **c-g**, **j**, and **l**: two-tailed simple linear regression; Pearson correlation coefficient (r). Panels **m** and **n**, unpaired one-tailed Student *t*-test.